

Are Anomaly Scores Telling the Whole Story? A Benchmark for Multilevel Anomaly Detection

Tri Cao¹, Minh-Huy Trinh^{3,4}, Ailin Deng¹, Quoc-Nam Nguyen¹, Khoa Duong²,
Ngai-Man Cheung², Bryan Hooi¹

¹National University of Singapore, ²Singapore University of Technology and Design,
³University of Science, ⁴Vietnam National University, Ho Chi Minh City.

Abstract

Anomaly detection (AD) is a machine learning task that identifies anomalies by learning patterns from normal training data. In many real-world scenarios, anomalies vary in severity, from minor anomalies with little risk to severe abnormalities requiring immediate attention. However, existing models primarily operate in a binary setting, and the anomaly scores they produce are usually based on the deviation of data points from normal data, which may not accurately reflect practical severity. In this paper, we address this gap by making three key contributions. First, we propose a novel setting, Multilevel AD (MAD), in which the anomaly score represents the severity of anomalies in real-world applications, and we highlight its diverse applications across various domains. Second, we introduce a novel benchmark, MAD-Bench, that evaluates models not only on their ability to detect anomalies, but also on how effectively their anomaly scores reflect severity. This benchmark incorporates multiple types of baselines and real-world applications involving severity. Finally, we conduct a comprehensive performance analysis on MAD-Bench. We evaluate models on their ability to assign severity-aligned scores, investigate the correspondence between their performance on binary and multilevel detection, and study their robustness. This analysis offers key insights into improving AD models for practical severity alignment. The code framework and datasets used for the benchmark will be made publicly available.

1. Introduction

Anomaly detection (AD) is a fundamental machine learning task that identifies deviations from normal patterns, with critical applications in domains such as one-class novelty detection [9, 40], industrial inspection [5, 69], and medical diagnostics [43, 47]. However, in many real-world scenarios, anomalies are not uniformly significant; they exist on

a spectrum of severity, ranging from minor anomalies that pose little risk to severe abnormalities that demand immediate attention. In a practical context, severity refers to the degree of potential impact or risk an anomaly poses to the system. For instance, in industrial inspection, as shown in Figure 1b, anomalies range from minor surface contaminations to severe tears, requiring different levels of response. The ability to differentiate between these levels of severity is important for effective decision-making, prioritizing critical issues, and resource allocation.

While distinguishing between different levels of anomaly severity is crucial, it remains unclear whether current anomaly detection methods are truly effective in capturing this distinction. Existing approaches typically focus on ensuring that the anomaly scores of anomalous data are higher than those of normal samples, operating primarily in a binary setting. Current techniques, such as reconstruction-based [36, 38, 57, 60, 63], one-class classifiers [9, 16, 41, 55, 58], and knowledge distillation-based models [12, 42, 49, 53], rely on metrics like reconstruction errors, distance measures, or likelihood estimates to flag deviations from normal patterns. However, the anomaly scores produced by these models are typically based on how far a data point deviates from normal data, but it is uncertain how well these scores correlate with the practical severity of the anomalies.

These observations raise a key question: How accurately can the anomaly scores measure practical severity? To the best of our knowledge, there are no works that directly address this question. While *near-distribution novelty detection* [34] is related, it focuses on distinguishing between normal samples and abnormal samples that closely resemble normal ones rather than investigating the relationship between anomaly scores and severity. In this paper, we aim to study the relationship between anomaly score and severity of anomalies by presenting three main contributions:

- First, we propose a novel setting, **Multilevel Anomaly Detection (MAD)**, where the anomaly score should represent the severity of anomalies in real-world appli-

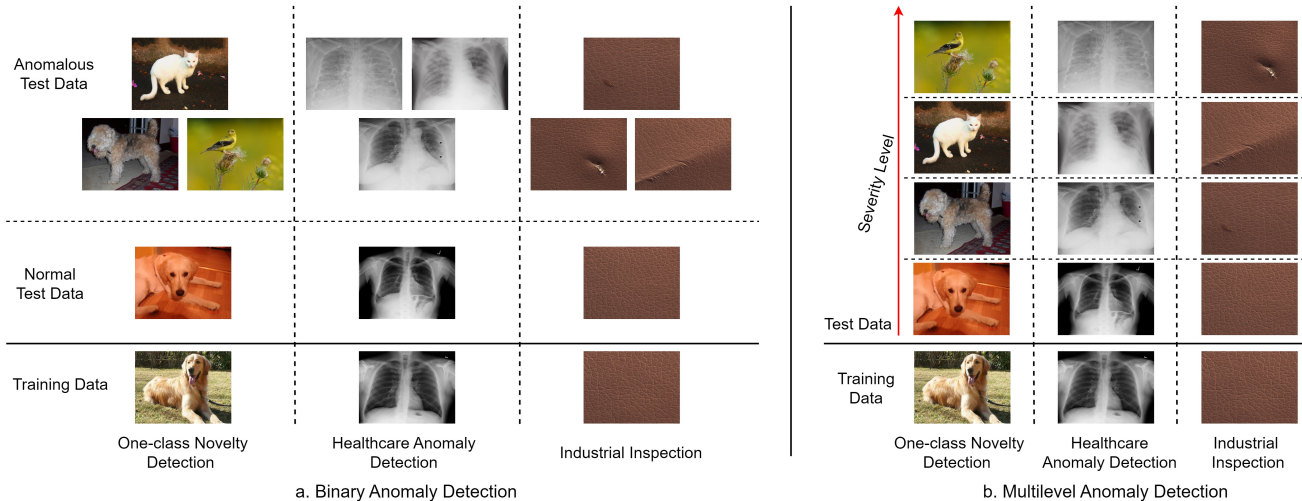


Figure 1. (a) Binary Anomaly Detection classifies data as either in-distribution (ID) or out-of-distribution (OOD), without accounting for severity. (b) The Multilevel Anomaly Detection setting categorizes OOD data by severity, reflecting the potential impact or risk. For instance, in COVID-19 chest X-rays, severity increases with greater lung involvement, from mild ground-glass opacities to extensive consolidation, indicating heightened clinical urgency.

cations. We highlight the applications of multilevel anomaly detection in real-world scenarios, including one-class novelty detection, anomaly detection in medical imaging, and industrial inspection.

- Building on the MAD setting, we introduce a new benchmark named **MAD-Bench**, designed to evaluate models on both their anomaly detection capabilities and their effectiveness in assigning severity-aligned anomaly scores. To achieve this, we adapt existing datasets from diverse domains to the multilevel anomaly detection context. In addition to conventional baselines, we incorporate Multimodal Large Language Model (MLLM)-based baselines, which leverage domain knowledge and reasoning abilities to assign anomaly scores. This makes MAD-Bench a comprehensive framework for evaluating model performance in MAD settings.
- Finally, we conduct a comprehensive performance analysis using MAD-Bench, evaluating models on their ability to assign severity-aligned anomaly scores, the correlation between binary and multilevel detection performance, and the impact of anomalous feature area. We also assess performance across severity levels, the effect of including light anomalies in the normal class, and robustness under input corruption. These insights help improve AD models for practical severity alignment.

2. Related Work

Traditional Approaches. Many approaches have been proposed for anomaly detection. One-class classification methods have progressed from machine learning approaches

[45, 48] to deep learning-based techniques [9, 16, 32, 40, 41, 55, 58], which improve boundary refinement for distinguishing normal and anomalous data. Reconstruction-based models [30, 38, 57, 60, 62–64] identify anomalies by measuring deviations in reconstruction errors. Additionally, self-supervised learning techniques [28, 44, 57, 67] introduce synthetic anomalies to enhance model differentiation, improving detection accuracy in complex scenarios. Knowledge distillation-based methods employ a teacher-student framework [6, 12, 17, 42, 49, 53, 66], where anomalies are detected based on deviations between teacher and student representations. Distribution map-based methods [18, 27, 46] model the normal data distribution and identify outliers as deviations. Memory-based approaches [4, 15, 17, 23, 36, 39, 53] detect anomalies by comparing input features to representative normal data stored in a memory bank.

MLLM-Based Approaches. MLLMs have recently been leveraged for anomaly detection due to their ability to handle multimodal reasoning. These approaches often utilize zero-shot learning [13, 24] or few-shot learning [29, 68], allowing them to adapt to new datasets without extensive task-specific training.

AD Benchmarks. Several benchmarks for anomaly detection have been introduced [3, 8, 19, 24, 52, 56, 65]. However, these benchmarks primarily focus on traditional binary anomaly detection rather than addressing more nuanced multilevel anomaly detection settings.

Near out-of-distribution (OOD) detection aims to identify anomalies that are similar to normal data, showing only slight deviations [34]. This differs from our work,

which explores the relationship between anomaly scores and varying levels of severity.

Multi-class AD identifies anomalies across various object classes within a single, unified framework [21, 33, 59, 65]. By training on multiple normal classes, it identifies anomalies as instances deviating from any learned normal patterns. In contrast, Multilevel AD focuses on representing multiple levels of anomalies during inference and ensures that anomaly scores reflect these levels.

3. Multilevel Anomaly Detection

3.1. Problem Formulation

In anomaly detection, the goal is to define a function $f : \mathcal{X} \rightarrow \mathbb{R}$ that assigns an anomaly score $f(x)$ to each data point $x \in \mathcal{X}$, where higher scores indicate a greater likelihood of being an anomaly. Traditional approaches typically treat anomalies in a binary manner, detecting whether a point is normal or anomalous. However, real-world anomalies often vary in severity rather than fitting into binary categories. For example, in medical diagnostics, doctors assess abnormalities on a spectrum, from mild issues needing observation to critical conditions requiring urgent care.

Motivated by this, we propose a *Multilevel Anomaly Detection (MAD)* setting, where data points are from L_0 to L_n , with L_0 representing the set of normal data and L_1, L_2, \dots, L_n representing sets of increasingly severe levels of anomaly.

Let the training set be defined as $\mathcal{D}_{\text{train}} \subseteq L_0$, consisting exclusively of normal data points from L_0 . The testing set is defined as $\mathcal{D}_{\text{test}} \subseteq L_0 \cup L_1 \cup \dots \cup L_n$, which includes data from all levels L_0, L_1, \dots, L_n .

The goal is to design an anomaly scoring function $f(x)$ such that higher severity levels correspond to higher anomaly scores. Specifically, normal data points in L_0 should be assigned the lowest anomaly scores $f(x_0)$, while data points from higher severity levels L_1, L_2, \dots, L_n should receive correspondingly higher scores. This ensures a consistent and interpretable mapping between anomaly severity and anomaly scores.

3.2. Evaluation Protocol

In this section, we outline the evaluation protocol used to assess the performance of models on the multi-level anomaly detection task. Three key metrics will be employed: **AUROC** [20], **C-index** [51], and **Kendall’s Tau-b** [25].

The AUROC metric is used to evaluate the model’s ability to distinguish between normal data and anomalies, which is commonly used in binary AD settings [8, 9].

The C-index is a generalization of the AUROC that can evaluate how well anomaly scores align with the severity

levels. In the context of MAD, C-index is defined as:

$$C = \frac{\sum_{a=1}^n \sum_{b=0}^{a-1} \sum_{x_i \in L_a} \sum_{x_j \in L_b} \mathbb{1}(f(x_i) > f(x_j))}{\sum_{a=1}^n \sum_{b=0}^{a-1} |L_a| \cdot |L_b|},$$

Similar to the AUROC, a C-index of 1 corresponds to the best model prediction, while a C-index of 0.5 indicates a random prediction. A high C-index score indicates that the model correctly ranks higher-severity anomalies with higher anomaly scores.

To further assess the alignment between predicted anomaly scores and severity levels, we employ Kendall’s Tau-b. Similar to C-index, Kendall’s Tau-b evaluates the consistency between anomaly scores and severity levels but is stricter, as it requires samples within the same severity level to have identical anomaly scores to ensure perfect agreement. Kendall’s Tau ranges from $[-1, 1]$, with -1 indicating a perfectly incorrect ranking, 0 signifying no correlation, and 1 representing a perfect severity ranking. The formula is detailed in the Appendix.

3.3. Applications of Multilevel Anomaly Detection

Multilevel anomaly detection has significant implications across real-world domains where distinguishing anomalies based on severity is essential for effective decision-making.

One-class Novelty Detection identifies samples that deviate from a defined normal class. For instance, a model trained on Golden Retriever (a dog breed) images can categorize anomalies by their deviation: Level 1 includes other dog breeds (minor deviation); Level 2, cats (moderate similarity); Level 3, birds (significant structural differences); and Level 4, flowers (inanimate objects). This framework enables one-class novelty detection to assign anomaly scores based on the degree of relevance to the trained class.

Medical Imaging often involves detecting and assessing anomalies that may significantly impact a patient’s health. Multilevel anomaly detection is valuable as it allows models to differentiate between conditions of varying severity. For instance, in a model trained on images of healthy skin, anomalies can be categorized into levels: Level 1 includes benign lesions, representing minor deviations with no immediate health risk; Level 2 encompasses precancerous lesions, indicating a moderate risk that requires monitoring or intervention; and Level 3 consists of cancerous lesions, severe anomalies demanding urgent medical attention. This structured detection enables healthcare professionals to prioritize high-risk cases, improving patient outcomes by addressing critical conditions promptly.

In **Industrial Inspection**, the economic and operational impact of anomalies can vary widely. Multilevel anomaly detection helps by assessing anomalies not just based on their physical characteristics, but also their potential economic or operational consequences. For example, a small

cosmetic defect on a non-essential part may be a low-severity anomaly, while a malfunction in a critical machine component that leads to production downtime or safety hazards would be classified as a high-severity anomaly. This approach ensures that high-risk anomalies that pose significant economic or safety threats are addressed first, optimizing quality control and manufacturing processes.

By applying multilevel anomaly detection, real-world applications across these domains benefit from more precise anomaly classification, which enables better prioritization and resource allocation.

4. MAD-Bench: Multilevel AD Benchmark

4.1. Datasets in MAD-Bench

Application	Dataset	Subset	Total Images	Number of Levels
Novelty Detection	MultiDogs-MAD	5	9500	5
Industrial Inspection	MVTec-MAD	14	5073	4
	VisA-MAD	9	7874	4
Medical Imaging	DRD-MAD	1	4500	5
	Covid19-MAD	1	1364	7
	SkinLesion-MAD	1	2469	4

Table 1. Summary of the six datasets used in MAD-Bench, comprising a total of 31 subsets included in the benchmark.

In our proposed benchmark, we evaluate anomaly detection models across various applications. Among the datasets used, two (DRD-MAD and Covid19-MAD) already include predefined severity labels. For the remaining datasets, which contain class labels for each sample. (e.g., defect types, disease types, or class names), we manually assign severity levels based on these class labels. Classes with ambiguity or samples that do not accurately reflect the assigned class name are excluded from the benchmark. Depending on the application, we categorize anomalies into different numbers of severity levels. The statistics of all datasets can be found in Table 1. Sample distribution across severity levels is detailed in the appendix.

4.1.1. One-Class Novelty Detection Datasets

We introduce the **MultiDogs-MAD** dataset to evaluate models’ ability to detect anomalies based on class similarity. The training set consists of 500 samples from each of five dog breeds selected from the Stanford Dogs Dataset [26]: Bichon Frise, Chinese Rural Dog, Golden Retriever, Labrador Retriever, and Teddy. Each breed in Level 0 is sequentially used as the normal class, with levels 1 to 4 as testing datasets introducing anomalies of increasing severity. Level 0 represents normal samples from the selected breed. Level 1 includes near-distribution anomalies from other dog breeds not in the training set, Level 2 introduces cat images as moderate anomalies [37], Level 3 includes bird images as high-severity anomalies [54], and Level 4 contains flower

images as the highest-severity anomalies [35], unrelated to animals. Each testing level contains 500 samples.

4.1.2. Industrial Inspection Datasets

Building on the MVTEC [5] and VisA [69] datasets, we create two MAD datasets, MVTEC-MAD and VisA-MAD, by assigning severity levels to anomalies based on the economic and operational impact of the class to which the anomalies belong. Classes that could not be confidently assigned a severity level were excluded. **MVTEC-MAD** includes over 5,073 high-resolution images across fourteen object and texture categories, with defect-free images for training and diverse defects in the test sets. **VisA-MAD** contains 7,874 images in nine subsets, with 6,405 for training and 1,469 for testing. Both datasets include four severity levels: Level 0 (non-defect), Level 1 (minor defects that are easily repairable), Level 2 (moderate defects with some economic impact), and Level 3 (severe defects with high economic impact).

4.1.3. Medical Datasets

The **DRD-MAD** is derived from the Diabetic Retinopathy Detection dataset [14], contains high-resolution retina images labeled on a 0-4 severity scale, where 0 represents no DR and 4 indicates proliferative DR. The images vary in quality and orientation due to different imaging conditions and camera models. For training, we randomly select 1000 normal samples (severity 0). Testing includes 700 samples for each severity level (0-4), ensuring balanced evaluation across all stages of the disease.

The **Covid19-MAD** is sourced from COVID-19 Severity Scoring [11], contains 1,364 chest X-ray images: 580 COVID-19 positive cases and 784 normal cases, with 703 images allocated for training. Severity scores for positive cases range from 0 (no findings) to 6 (severe, above 85% lung involvement), sourced from four public datasets and annotated by two independent radiologists.

The **SkinLesion-MAD** is designed to evaluate models in detecting and classifying skin anomalies across varying severity levels. It includes 500 training and 500 testing images of healthy skin sourced from Kaggle [1]. Anomalous images from the ISIC Challenge 2018 dataset [10, 50], labeled by two doctors through consensus, are divided into Benign lesions (e.g., Melanocytic nevus, Vascular lesions, 652 samples), Precancerous lesions (Actinic keratosis, 327 samples), and Cancerous lesions (Melanoma, 500 samples).

4.2. Conventional Baselines

We include baselines of several types, including one-class classification, knowledge distillation-based, reconstruction-based, memory-bank, and distribution map-based methods. The methods we evaluate are Skip-GAN [2], OCR-GAN [31], AE4AD [7], IGD [9], RD4AD [12], RRD [49], PatchCore [39], PNI [4], CFLOW-AD [18] and SPR [46]. The

details are in Table 2.

For all baselines, we strictly follow the original settings, including all hyperparameters such as the learning rate, number of training epochs, optimizer, and others. For new datasets, we apply baseline settings from similar datasets. For each model, we derive the sample-level anomaly score based on its design and use it to evaluate performance.

Type	Method	Year
Reconstruction	Skip-GAN [2]	2019
	OCR-GAN [31]	2023
	AE4AD [7]	2024
Knowledge Distillation	RD4AD [12]	2022
	RRD [49]	2023
Memory-bank	PatchCore [39]	2022
	PNI [4]	2023
One-class Classification	IGD [9]	2022
Distribution Map	CFLOW-AD [18]	2022
	SPR [46]	2023
MLLMs	MMAD-4o	Ours
	MMAD-4o-mini	Ours
	MMAD-Sonnet	Ours
	MMAD-Haiku	Ours

Table 2. Summary of conventional baselines by approach type.

4.3. MLLM-based Baselines

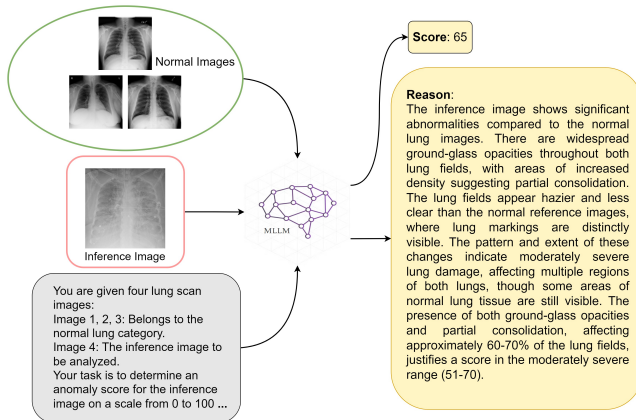


Figure 2. MLLM-based baselines enable few-shot multilevel AD by leveraging their domain knowledge without fine-tuning, unlike conventional baselines requiring target data training.

We acknowledge that assigning anomaly scores corresponding to severity levels requires domain knowledge, which conventional baselines lack. Researchers have recently explored MLLMs for zero-shot learning [13, 24] or few-shot learning [29, 68], but these methods do not include the specific context of multilevel anomaly detection. Thus, we introduce MLLM-based baselines tailored to the MAD setting. We adopt a few-shot setting to balance effectiveness and cost, by utilizing four images: three normal images and one inference image. We prompt the model with the neces-

sary application context, and instruct it to compare the inference image with the normal images. Based on this comparison, the model generates an anomaly score ranging from 0 to 100, accompanied by reasons, with higher scores indicating greater severity. Figure 2 illustrates the overall framework. We evaluate the approach using four state-of-the-art MLLMs: GPT-4o, GPT-4o-mini, Claude-3.5-Sonnet, and Claude-3.0-Haiku. Additional details on the experimental setup and prompts are provided in the appendix.

5. Experiments and Analysis on MAD-Bench

5.1. Research Questions

We conduct experiments to answer the research questions:

- **RQ1: (Benchmark and Model Types Analysis)** How accurately can different types of anomaly detection models assign anomaly scores that align with severity levels across various applications?
- **RQ2: (Binary-Multilevel Performance Correlation)** Does a model that performs well in binary anomaly detection also perform well in multilevel anomaly detection?
- **RQ3: (Anomalous Area Effect)** How does the area of anomalies affect their anomaly score?
- **RQ4: (Detection Performance Across Severity)** How does binary detection performance vary across different severity levels of anomalies?
- **RQ5: (Normal Class Expansion)** How do the models perform when light anomalies are considered acceptable and included as part of the normal class?
- **RQ6: (Robustness Analysis)** How robust are detection models in aligning anomaly scores with severity under data corruption?

5.2. RQ1: Benchmark and Model Type Analysis

We conducted a comprehensive benchmark across six datasets: MultiDogs-MAD, MVTec-MAD, VisA-MAD, DRD-MAD, Covid19-MAD, and SkinLesion-MAD, evaluating models on three metrics: AUROC (binary AD), C-index, and Kendall’s Tau-b. Table 3 shows results averaged across dataset subsets. Detailed results are in the appendix.

Conventional models perform reasonably well in multilevel AD tasks on four datasets: MultiDogs-MAD, MVTec-MAD, Visa-MAD, and SkinLesion-MAD, with state-of-the-art methods achieving C scores above 80%. However, these models struggle on the two medical datasets, DRD-MAD and Covid19-MAD, where C scores are around 65%. This suggests that multilevel AD for medical images, such as X-rays and retinal fundus images, presents greater challenges for conventional models. Among conventional approaches, knowledge distillation (e.g., RRD, RD4AD) and memory bank-based methods (e.g., PatchCore, PNI) demonstrated higher overall performance. Other approaches, particularly reconstruction-based models, show

Method	MultiDogs-MAD			MVTec-MAD			VisA-MAD			DRD-MAD			Covid19-MAD			SkinLesion-MAD			Average			Average Rank		
	AUC	Ken	C	AUC	Ken	C	AUC	Ken	C	AUC	Ken	C	AUC	Ken	C	AUC	Ken	C	AUC	Ken	C	AUC	Ken	C
Skip-GAN [2]	87.37	0.541	80.25	57.75	0.057	53.35	82.64	0.487	80.29	51.36	0.014	50.77	68.50	0.006	50.34	99.60	0.406	73.65	74.54	0.252	64.78	11	12	11
OCR-GAN [31]	75.63	0.343	69.19	94.39	0.401	73.90	91.17	0.526	83.03	53.83	0.054	53.03	65.46	0.038	52.09	99.53	0.391	72.76	80.00	0.292	67.33	10	11	9
AE4AD [7]	48.54	0.064	46.43	71.48	0.259	65.41	76.08	0.365	72.88	49.66	0.029	51.63	74.45	0.189	60.26	99.13	0.505	79.42	69.89	0.214	62.67	13	13	12
RD4AD [12]	67.44	0.308	67.20	98.92	0.504	79.86	95.24	0.640	89.79	61.30	0.217	62.14	83.48	0.219	61.90	98.94	0.509	79.60	84.22	0.399	73.41	8	7	6
RRD [49]	81.67	0.510	78.51	99.51	0.518	80.72	93.99	0.620	88.53	61.83	0.243	63.55	84.36	0.240	63.07	99.53	0.558	82.48	86.81	0.448	76.14	4	4	3
PatchCore [39]	75.71	0.410	72.94	99.11	0.512	80.36	93.32	0.602	87.42	61.36	0.259	64.47	76.33	0.200	60.88	100.0	0.456	76.57	84.31	0.407	73.77	6	6	5
PNI [4]	77.20	0.413	73.11	99.32	0.487	78.91	96.07	0.622	88.64	62.50	0.285	65.94	87.96	0.241	63.12	100.0	0.455	76.51	87.17	0.417	74.37	2	5	4
IGD [9]	95.02	0.424	73.67	87.67	0.384	72.78	79.34	0.419	75.94	54.33	0.170	59.51	85.82	0.312	66.99	97.91	0.487	78.34	83.35	0.366	71.20	9	10	8
CFLOW-AD [18]	89.45	0.431	74.11	96.79	0.466	77.58	85.08	0.493	80.43	60.21	0.238	63.30	74.03	0.180	59.78	99.98	0.389	72.63	84.26	0.366	71.30	7	9	7
SPR [46]	64.29	0.242	63.55	97.76	0.451	76.78	56.05	0.087	55.49	46.32	0.003	48.11	55.14	0.006	53.51	91.31	0.335	69.50	68.48	0.191	61.16	14	14	13
MMAD-4o	98.44	0.933	95.91	95.98	0.646	83.52	79.34	0.621	77.74	65.80	0.433	67.72	88.07	0.547	76.94	99.43	0.694	85.61	87.85	0.646	81.24	1	1	1
MMAD-4o-mini	98.27	0.743	80.35	93.45	0.614	81.89	76.44	0.500	74.06	63.55	0.348	66.66	79.58	0.351	66.98	99.75	0.653	84.97	85.17	0.535	75.82	5	3	4
MMAD-Sonnet	97.89	0.936	97.34	90.02	0.557	77.33	76.24	0.561	74.86	65.02	0.403	69.30	92.35	0.601	80.54	99.82	0.610	79.23	86.89	0.611	79.77	3	2	2
MMAD-Haiku	93.03	0.767	88.55	76.10	0.366	66.63	61.81	0.326	60.43	53.39	0.125	56.20	59.42	0.142	54.16	99.85	0.479	74.19	73.93	0.367	66.69	12	8	10

Table 3. Multilevel AD performance comparison across six datasets. The results are averaged across all subsets of each dataset. Higher AUROC (AUC) (%), Kendall’s Tau-b (Ken), and C-index (C) (%) values indicate better performance. A lower average rank reflects better overall results based on the average scores for each metric. **RED**: Best MLLM-based baseline. **BLUE**: Best conventional baseline. (RQ1-2)

lower performance in both binary detection and severity level alignment.

Most MLLM-based models (except MMAD-Haiku) demonstrated consistently better performance than conventional methods across all datasets, except the VisA-MAD dataset. They achieved both high AUC values and stronger alignment between anomaly scores and severity levels. For instance, in MultiDogs-MAD, MVTec-MAD and SkinLesion-MAD, these models not only matched conventional models in binary detection but also excelled in severity differentiation, as reflected in higher C and Ken values. A notable challenge is observed with the DRD-MAD dataset, which focuses on diabetic retinopathy detection. This dataset is particularly difficult for all models due to its requirement for expert-level knowledge to accurately assess severity levels.

Generally, most MLLM-based models outperformed conventional models in multilevel anomaly detection by effectively leveraging domain knowledge, multimodal reasoning, and contextual information to better understand anomaly characteristics and severity.

Finding 1: Among conventional methods, knowledge distillation and memory bank-based methods better align anomaly scores with severity levels. However, MLLM-based models further outperform these methods, highlighting the importance of prior knowledge in multilevel anomaly detection.

5.3. RQ2: Binary-Multilevel Performance Correlation

Since most prior evaluations in anomaly detection focus on the binary setting, we investigate how model performance under the binary setting correlates with performance under our proposed multilevel setting. To this end, we compute

the average scores for each metric across all datasets and rank the baselines accordingly, as shown in Table 3 (a lower average rank indicates better performance). We then calculate Spearman correlation coefficients [61] of 0.973 between AUC and C, and 0.916 between AUC and Ken, indicating a strong positive correlation between binary and multilevel performance metrics.

However, despite this overall strong correlation, certain models exhibit notable discrepancies. For most models, the rank differences between AUC and Ken or AUC and C remain within 2, but MMAD-Haiku shows a rank difference of 4, and PNI has a difference of 3. Besides, the binary detection rankings of MLLM-based baselines are consistently higher (worse) than their multilevel detection rankings. This suggests that while MLLM-based models excel in aligning anomaly scores with severity levels (multilevel detection), their binary anomaly detection performance is comparatively weaker. These observations show that binary evaluation does not fully reflect multilevel performance, underscoring the need for our benchmark.

Finding 2: Binary and multilevel detection metrics generally correlate, but some models, notably MLLM-based baselines, perform better in multilevel evaluation.

5.4. RQ3: Anomalous Area Effect

We hypothesize that the area of the anomalous region may affect the anomaly score generated by detection models, as these models often rely on differences in spatial features to identify anomalies. To validate this hypothesis, we conduct experiments using the MVTec-MAD and VisA-MAD datasets, as both include ground truth masks for the anomalies. The masks are resized to a width of 256 pixels while maintaining the aspect ratio. We then calculate the anomaly

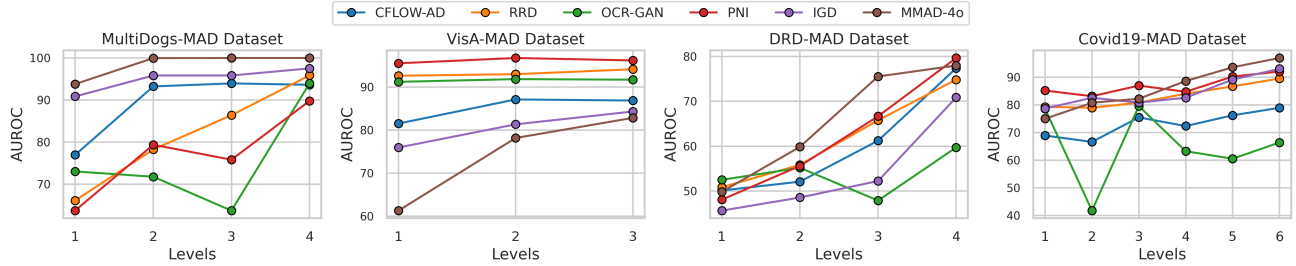


Figure 3. Binary AD performance across severity levels. An upward trend is observed in most models (RQ4).

Model	MVTec-MAD		ViSA-MAD	
	Risk-based	Area-based	Risk-based	Area-based
OCR-GAN	73.90	85.85	83.03	86.76
RD4AD	79.08	86.84	89.79	92.29
RRD	80.72	87.18	88.53	91.41
PatchCore	80.36	87.18	87.42	90.71
PNI	78.91	88.75	88.64	92.90
IGD	72.80	83.86	75.94	77.84
CFLOW-AD	77.58	86.64	80.43	83.27
MMAD-4o	83.52	89.05	77.74	78.17
MMAD-4o-mini	81.89	84.60	74.06	74.24
MMAD-Sonnet	77.33	82.73	74.86	75.11

Table 4. Risk-based and Area-based performance comparison is reported in C-index (%). Conventional methods tend to be biased toward larger anomalous areas (RQ3).

area for each sample and use it as the basis for defining an area-based severity level.

Table 4 presents the multilevel anomaly detection performance for both risk-based severity levels (as used in our benchmark) and area-based severity levels. The experimental results indicate a strong correlation between the area of anomalous regions and anomaly scores. This is evidenced by the C values for area-based severity levels, which consistently exceed 80% and are always higher than the C values for risk-based severity levels across both MVTec-MAD and VisA-MAD, with the exception of the MLLM-based baselines. Notably, models such as RD4AD, PatchCore, RRD, and PNI achieve exceptionally high C scores on VisA. These results suggest a bias in conventional models toward the area of anomalous regions.

This bias can be advantageous in applications where severity levels are strongly correlated with the area of anomalous regions, such as surface scratches, where a larger area generally indicates greater severity. However, it can underestimate the severity of anomalies with small areas but significant impact, such as a severed electrical wire.

Finding 3: Conventional models are biased toward larger spatial anomalies, assigning them higher scores, while MLLMs show less of this tendency.

5.5. RQ4: Detection Performance Across Severity

A more severe anomaly is intuitively more noticeable to humans. We investigate whether models follow this intuition by examining their performance across increasing severity levels. Specifically, we calculate the AUC between the normal class and each severity level. Results are reported only for MultiDogs-MAD, VisA-MAD, DRD-MAD, and Covid19-MAD in Figure 3, as performance on MVTec-MAD and SkinLesion-MAD is nearly flawless across all severity levels. Generally, most models exhibit an upward trend in detection performance as severity levels increase, indicating that higher-severity anomalies are detected more effectively. However, this trend is inconsistent at adjacent lower levels. Specifically, while the performance of most models at the highest levels across all datasets consistently surpasses that at lower levels, models such as PNI and OCR-GAN show inconsistencies in achieving better performance as the severity level increases at adjacent lower levels (e.g., Levels 1, 2, and 3).

Finding 4: Most models detect higher-severity anomalies more effectively. Yet, fluctuations are observed at lower severity levels in certain cases.

5.6. RQ5: Normal Class Expansion

In practice, light anomalies are often considered acceptable and may be treated as part of the normal class. For example, a model trained on images of healthy skin without any abnormalities might encounter an inference image with a benign mole, which users want to consider as normal. To replicate this, during test time, we expand the definition of the normal class by progressively including samples from abnormal classes as normal based on severity levels. It is important to note that during the training phase, we exclusively use normal samples (level 0).

Figure 4 shows that all models experience a performance decline as the normal class expands to include light anomalies, except for MMAD-4o, which maintains stability on several datasets. This decline occurs because many models assign similarly high anomaly scores to light and serious

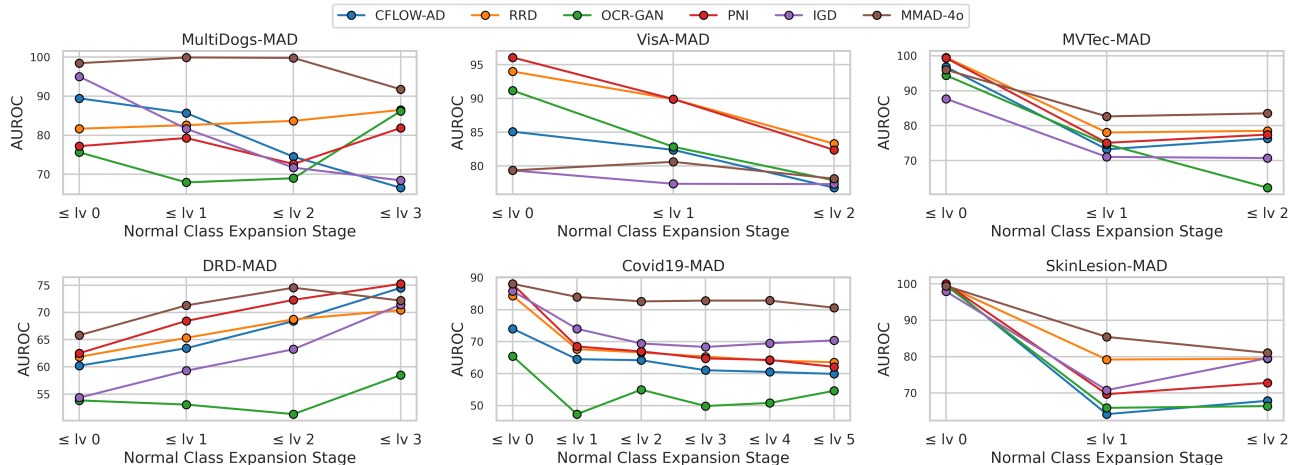


Figure 4. Performance changes under expansions of the normal class definition. “ \leq lv i ” means that we consider the classes with severity levels no more than i as normal classes in test time. Most models cannot maintain consistent performance across most datasets (RQ5).

anomalies, hindering adaptation to the expanded normal class. MMAD-4o’s robustness stems from its ability to distinguish between light and severe anomalies. For DRD-MAD, the upward trend is due to the nature of light anomalies, which are difficult to distinguish from normal samples. Models often assign low anomaly scores to these anomalies, treating them as normal. This behavior allows models to adapt more effectively when light anomalies are included in the normal class, maintaining detection performance.

Finding 5: All models experience a drop in performance when light anomalies are considered as normal samples, but MLLMs have a smaller drop.

ruption having a particularly strong effect on MVTec-MAD and SkinLesion-MAD. This is because noise can be misinterpreted by the models as defects, leading to a significant drop in C-index. In contrast, models evaluated on the MultiDogs-MAD are less affected by both types of corruption, due to the dataset’s characteristic as a one-class novelty detection application, which encourages the models to rely on abstract features rather than fine-grained features.

Finding 6: All models are negatively affected by corruption, particularly on datasets requiring fine-grained feature analysis.

5.7. RQ6: Robustness Analysis

Model	MultiDogs-MAD			MVTec-MAD			SkinLesion-MAD		
	Orig	Brgt	Noise	Orig	Brgt	Noise	Orig	Brgt	Noise
OCR-GAN	69.19	66.70	68.08	73.90	69.33	67.23	72.76	70.02	63.38
RRD	78.51	77.99	73.70	80.72	77.60	73.61	82.48	80.46	48.40
PatchCore	72.94	73.40	69.41	80.36	78.91	78.66	76.57	75.86	70.75
PNI	73.11	73.21	71.77	78.91	75.32	67.70	76.51	73.83	70.29
IGD	73.67	68.70	71.59	72.78	65.91	65.91	78.34	80.44	67.55
CFLOW-AD	74.11	72.44	69.41	77.58	67.02	63.48	72.63	70.43	68.13
MMAD-4o	95.91	94.28	94.71	83.52	79.00	72.82	85.61	80.91	54.72
MMAD-Sonnet	97.34	96.19	95.04	77.33	73.64	67.16	79.23	77.33	67.43

Table 5. Performance comparison on brightness (Brgt), Gaussian noise (Noise), and origin (Orig) using C-index (%). All models are adversely affected by corruption (RQ6).

To evaluate the robustness of anomaly detection models under corrupted input data, we use C-index on three datasets (MultiDogs-MAD, MVTec-MAD, and SkinLesion-MAD) under two types of input corruptions [8, 22]: brightness adjustment and noise addition. Table 5 shows that all models are negatively impacted by corruption, with noise cor-

6. Future Direction

A promising direction for multilevel anomaly detection lies in integrating MLLMs with conventional approaches to leverage their complementary strengths. MLLMs excel in aligning anomaly scores with severity levels through domain knowledge and contextual reasoning, while conventional models perform better in binary detection, particularly for industrial inspection. A hybrid approach, such as a two-stage framework where conventional models detect anomalies and MLLMs assign severity scores, offers a robust and comprehensive solution by combining high accuracy in detection with contextual understanding for severity assessment.

7. Conclusion

In this paper, we introduce Multilevel Anomaly Detection (MAD), a novel setting that emphasizes the alignment of anomaly scores with practical severity. To support this setting, we develop MAD-Bench, a comprehensive benchmark

that evaluates the ability of models to reflect severity in diverse real-world applications. Through extensive analysis, we provide various findings, revealing insights into the relationship between binary and multilevel detection performance, as well as model robustness. These contributions highlight the potential for MAD to bridge the gap between theoretical anomaly detection and its practical deployment, paving the way for more effective and context-aware AD systems in real-world domains.

References

- [1] Ahdasdwdasd. Our-normal-skin, 2023. 4
- [2] Samet Akçay, Amir Atapour-Abarghouei, and Toby P Breckon. Skip-ganomaly: Skip connected and adversarially trained encoder-decoder anomaly detection. In *2019 International Joint Conference on Neural Networks (IJCNN)*, pages 1–8. IEEE, 2019. 4, 5, 6, 12, 13, 14, 15, 16, 17, 18
- [3] Samet Akçay, Dick Ameln, Ashwin Vaidya, Barath Lakshmanan, Nilesh Ahuja, and Utku Genc. Anomalib: A deep learning library for anomaly detection. In *2022 IEEE International Conference on Image Processing (ICIP)*, pages 1706–1710. IEEE, 2022. 2
- [4] Jaehyeok Bae, Jae-Han Lee, and Seyun Kim. Pni: Industrial anomaly detection using position and neighborhood information. In *Proceedings of the IEEE/CVF International Conference on Computer Vision*, pages 6373–6383, 2023. 2, 4, 5, 6, 12, 13, 14, 15, 16, 17, 18
- [5] Paul Bergmann, MiFchael Fauser, David Sattlegger, and Carsten Steger. Mvtec ad—a comprehensive real-world dataset for unsupervised anomaly detection. In *Proceedings of the IEEE/CVF conference on computer vision and pattern recognition*, pages 9592–9600, 2019. 1, 4
- [6] Paul Bergmann, Michael Fauser, David Sattlegger, and Carsten Steger. Uninformed students: Student-teacher anomaly detection with discriminative latent embeddings. In *Proceedings of the IEEE/CVF conference on computer vision and pattern recognition*, pages 4183–4192, 2020. 2
- [7] Yu Cai, Hao Chen, and Kwang-Ting Cheng. Rethinking autoencoders for medical anomaly detection from a theoretical perspective. *arXiv preprint arXiv:2403.09303*, 2024. 4, 5, 6, 12, 13, 14, 15, 16, 17, 18
- [8] Tri Cao, Jiawen Zhu, and Guansong Pang. Anomaly detection under distribution shift. In *Proceedings of the IEEE/CVF International Conference on Computer Vision*, pages 6511–6523, 2023. 2, 3, 8
- [9] Yuanhong Chen, Yu Tian, Guansong Pang, and Gustavo Carneiro. Deep one-class classification via interpolated gaussian descriptor. In *Proceedings of the AAAI Conference on Artificial Intelligence*, pages 383–392, 2022. 1, 2, 3, 4, 5, 6, 12, 13, 14, 15, 16, 17, 18
- [10] Noel Codella, Veronica Rotemberg, Philipp Tschandl, M Emre Celebi, Stephen Dusza, David Gutman, Brian Helba, Aadi Kalloo, Konstantinos Liopyris, Michael Marchetti, et al. Skin lesion analysis toward melanoma detection 2018: A challenge hosted by the international skin imaging collaboration (isic). *arXiv preprint arXiv:1902.03368*, 2019. 4
- [11] VV Danilov, Alex Proutski, Alexander Kirpich, DE Litmanovich, and Yuriy Gankin. Dataset for covid-19 segmentation and severity scoring. *Mendeley Data*, 10, 2022. 4
- [12] Hanqiu Deng and Xingyu Li. Anomaly detection via reverse distillation from one-class embedding. In *Proceedings of the IEEE/CVF Conference on Computer Vision and Pattern Recognition*, pages 9737–9746, 2022. 1, 2, 4, 5, 6, 12, 13, 14, 15, 16, 17, 18
- [13] Hanqiu Deng, Zhaoxiang Zhang, Jinan Bao, and Xingyu Li. Anovl: Adapting vision-language models for unified zero-shot anomaly localization. *arXiv preprint arXiv:2308.15939*, 2023. 2, 5
- [14] Emma Dugas, Jared Jorge, and Will Cukierski. Diabetic retinopathy detection. <https://kaggle.com/competitions/diabetic-retinopathy-detection>, 2015. Kaggle. 4
- [15] Dong Gong, Lingqiao Liu, Vuong Le, Budhaditya Saha, Moussa Reda Mansour, Svetha Venkatesh, and Anton van den Hengel. Memorizing normality to detect anomaly: Memory-augmented deep autoencoder for unsupervised anomaly detection. In *Proceedings of the IEEE/CVF International Conference on Computer Vision*, pages 1705–1714, 2019. 2
- [16] Sachin Goyal, Aditi Raghunathan, Moksh Jain, Harsha Vardhan Simhadri, and Prateek Jain. Drocc: Deep robust one-class classification. In *International conference on machine learning*, pages 3711–3721. PMLR, 2020. 1, 2
- [17] Zhihao Gu, Liang Liu, Xu Chen, Ran Yi, Jiangning Zhang, Yabiao Wang, Chengjie Wang, Annan Shu, Guannan Jiang, and Lizhuang Ma. Remembering normality: Memory-guided knowledge distillation for unsupervised anomaly detection. In *Proceedings of the IEEE/CVF International Conference on Computer Vision*, pages 16401–16409, 2023. 2
- [18] Denis Gudovskiy, Shun Ishizaka, and Kazuki Kozuka. Cflow-ad: Real-time unsupervised anomaly detection with localization via conditional normalizing flows. In *Proceedings of the IEEE/CVF winter conference on applications of computer vision*, pages 98–107, 2022. 2, 4, 5, 6, 12, 13, 14, 15, 16, 17, 18
- [19] Songqiao Han, Xiyang Hu, Hailiang Huang, Minqi Jiang, and Yue Zhao. Adbench: Anomaly detection benchmark. *Advances in Neural Information Processing Systems*, 35: 32142–32159, 2022. 2
- [20] James A Hanley and Barbara J McNeil. The meaning and use of the area under a receiver operating characteristic (roc) curve. *Radiology*, 143(1):29–36, 1982. 3, 1
- [21] Haoyang He, Jiangning Zhang, Hongxu Chen, Xuhai Chen, Zhishan Li, Xu Chen, Yabiao Wang, Chengjie Wang, and Lei Xie. A diffusion-based framework for multi-class anomaly detection. In *Proceedings of the AAAI Conference on Artificial Intelligence*, pages 8472–8480, 2024. 3
- [22] Dan Hendrycks and Thomas Dietterich. Benchmarking neural network robustness to common corruptions and perturbations. *Proceedings of the International Conference on Learning Representations*, 2019. 8
- [23] Jinlei Hou, Yingying Zhang, Qiaoyong Zhong, Di Xie, Shiliang Pu, and Hong Zhou. Divide-and-assemble: Learning

- block-wise memory for unsupervised anomaly detection. In *Proceedings of the IEEE/CVF International Conference on Computer Vision*, pages 8791–8800, 2021. 2
- [24] Xi Jiang, Jian Li, Hanqiu Deng, Yong Liu, Bin-Bin Gao, Yifeng Zhou, Jialin Li, Chengjie Wang, and Feng Zheng. Mmad: The first-ever comprehensive benchmark for multimodal large language models in industrial anomaly detection. 2024. 2, 5
- [25] Maurice G Kendall. A new measure of rank correlation. *Biometrika*, 30(1-2):81–93, 1938. 3, 1
- [26] Aditya Khosla, Nityananda Jayadevaprakash, Bangpeng Yao, and Li Fei-Fei. Novel dataset for fine-grained image categorization. In *First Workshop on Fine-Grained Visual Categorization, IEEE Conference on Computer Vision and Pattern Recognition*, Colorado Springs, CO, 2011. 4
- [27] Jiarui Lei, Xiaobo Hu, Yue Wang, and Dong Liu. Pyramid-flow: High-resolution defect contrastive localization using pyramid normalizing flow. In *Proceedings of the IEEE/CVF Conference on Computer Vision and Pattern Recognition (CVPR)*, pages 14143–14152, 2023. 2
- [28] Chun-Liang Li, Kihyuk Sohn, Jinsung Yoon, and Tomas Pfister. Cutpaste: Self-supervised learning for anomaly detection and localization. In *Proceedings of the IEEE/CVF Conference on Computer Vision and Pattern Recognition*, pages 9664–9674, 2021. 2
- [29] Xiaofan Li, Zhizhong Zhang, Xin Tan, Chengwei Chen, Yanyun Qu, Yuan Xie, and Lizhuang Ma. Promptad: Learning prompts with only normal samples for few-shot anomaly detection. In *Proceedings of the IEEE/CVF Conference on Computer Vision and Pattern Recognition*, pages 16838–16848, 2024. 2, 5
- [30] Yufei Liang, Jiangning Zhang, Shiwei Zhao, Runze Wu, Yong Liu, and Shuwen Pan. Omni-frequency channel-selection representations for unsupervised anomaly detection. *arXiv preprint arXiv:2203.00259*, 2022. 2
- [31] Yufei Liang, Jiangning Zhang, Shiwei Zhao, Runze Wu, Yong Liu, and Shuwen Pan. Omni-frequency channel-selection representations for unsupervised anomaly detection. *IEEE Transactions on Image Processing*, 2023. 4, 5, 6, 12, 13, 14, 15, 16, 17, 18
- [32] Zhikang Liu, Yiming Zhou, Yuansheng Xu, and Zilei Wang. Simplenet: A simple network for image anomaly detection and localization. In *Proceedings of the IEEE/CVF Conference on Computer Vision and Pattern Recognition*, pages 20402–20411, 2023. 2
- [33] Ruiying Lu, YuJie Wu, Long Tian, Dongsheng Wang, Bo Chen, Xiyang Liu, and Ruimin Hu. Hierarchical vector quantized transformer for multi-class unsupervised anomaly detection. *Advances in Neural Information Processing Systems*, 36:8487–8500, 2023. 3
- [34] Hossein Mirzaei, Mohammadreza Salehi, Sajjad Shahabi, Efstratios Gavves, Cees GM Snoek, Mohammad Sabokrou, and Mohammad Hossein Rohban. Fake it until you make it: Towards accurate near-distribution novelty detection. In *The Eleventh International Conference on Learning Representations*, 2022. 1, 2
- [35] Maria-Elena Nilsback and Andrew Zisserman. Automated flower classification over a large number of classes. In *International Conference on Computer Vision, Graphics and Image Processing*, 2008. 4
- [36] Hyunjong Park, Jongyouon Noh, and Bumsub Ham. Learning memory-guided normality for anomaly detection. In *Proceedings of the IEEE/CVF conference on computer vision and pattern recognition*, pages 14372–14381, 2020. 1, 2
- [37] Omkar M Parkhi, Andrea Vedaldi, Andrew Zisserman, and C. V. Jawahar. Cats and dogs. In *2012 IEEE Conference on Computer Vision and Pattern Recognition*, pages 3498–3505, 2012. 4
- [38] Masoud Pourreza, Bahram Mohammadi, Mostafa Khaki, Samir Bouindour, Hichem Snoussi, and Mohammad Sabokrou. G2d: Generate to detect anomaly. In *Proceedings of the IEEE/CVF Winter Conference on Applications of Computer Vision*, pages 2003–2012, 2021. 1, 2
- [39] Karsten Roth, Latha Pemula, Joaquin Zepeda, Bernhard Schölkopf, Thomas Brox, and Peter Gehler. Towards total recall in industrial anomaly detection. In *Proceedings of the IEEE/CVF conference on computer vision and pattern recognition*, pages 14318–14328, 2022. 2, 4, 5, 6, 12, 13, 14, 15, 16, 17, 18
- [40] Lukas Ruff, Robert Vandermeulen, Nico Goernitz, Lucas Deecke, Shoaib Ahmed Siddiqui, Alexander Binder, Emmanuel Müller, and Marius Kloft. Deep one-class classification. In *International conference on machine learning*, pages 4393–4402. PMLR, 2018. 1, 2
- [41] Mohammad Sabokrou, Mahmood Fathy, Guoying Zhao, and Ehsan Adeli. Deep end-to-end one-class classifier. *IEEE transactions on neural networks and learning systems*, 32(2):675–684, 2020. 1, 2
- [42] Mohammadreza Salehi, Niousha Sadjadi, Soroosh Baselizadeh, Mohammad H Rohban, and Hamid R Rabiee. Multiresolution knowledge distillation for anomaly detection. In *Proceedings of the IEEE/CVF conference on computer vision and pattern recognition*, pages 14902–14912, 2021. 1, 2
- [43] Thomas Schlegl, Philipp Seeböck, Sebastian M Waldstein, Georg Langs, and Ursula Schmidt-Erfurth. f-anogan: Fast unsupervised anomaly detection with generative adversarial networks. *Medical image analysis*, 54:30–44, 2019. 1
- [44] Hannah M Schlüter, Jeremy Tan, Benjamin Hou, and Bernhard Kainz. Natural synthetic anomalies for self-supervised anomaly detection and localization. In *European Conference on Computer Vision*, pages 474–489. Springer, 2022. 2
- [45] Bernhard Schölkopf, John C Platt, John Shawe-Taylor, Alex J Smola, and Robert C Williamson. Estimating the support of a high-dimensional distribution. *Neural computation*, 13(7):1443–1471, 2001. 2
- [46] Woosang Shin, Jonghyeon Lee, Taehan Lee, Sangmoon Lee, and Jong Pil Yun. Anomaly detection using score-based perturbation resilience. In *Proceedings of the IEEE/CVF International Conference on Computer Vision*, pages 23372–23382, 2023. 2, 4, 5, 6, 12, 13, 14, 15, 16, 17, 18
- [47] Nina Shvetsova, Bart Bakker, Irina Fedulova, Heinrich Schulz, and Dmitry V Dyllov. Anomaly detection in medical imaging with deep perceptual autoencoders. *IEEE Access*, 9: 118571–118583, 2021. 1

- [48] David MJ Tax and Robert PW Duin. Support vector data description. *Machine learning*, 54:45–66, 2004. [2](#)
- [49] Tran Dinh Tien, Anh Tuan Nguyen, Nguyen Hoang Tran, Ta Duc Huy, Soan Duong, Chanh D Tr Nguyen, and Steven QH Truong. Revisiting reverse distillation for anomaly detection. In *Proceedings of the IEEE/CVF conference on computer vision and pattern recognition*, pages 24511–24520, 2023. [1](#), [2](#), [4](#), [5](#), [6](#), [12](#), [13](#), [14](#), [15](#), [16](#), [17](#), [18](#)
- [50] Philipp Tschandl, Cliff Rosendahl, and Harald Kittler. The ham10000 dataset, a large collection of multi-source dermatoscopic images of common pigmented skin lesions. *Scientific data*, 5(1):1–9, 2018. [4](#)
- [51] Hajime Uno, Tianxi Cai, Michael J Pencina, Ralph B D’Agostino, and Lee-Jen Wei. On the c-statistics for evaluating overall adequacy of risk prediction procedures with censored survival data. *Statistics in medicine*, 30(10):1105–1117, 2011. [3](#), [1](#)
- [52] Chengjie Wang, Wenbing Zhu, Bin-Bin Gao, Zhenye Gan, Jiangning Zhang, Zhihao Gu, Shuguang Qian, Mingang Chen, and Lizhuang Ma. Real-ia-d: A real-world multi-view dataset for benchmarking versatile industrial anomaly detection. In *Proceedings of the IEEE/CVF Conference on Computer Vision and Pattern Recognition*, pages 22883–22892, 2024. [2](#)
- [53] Guodong Wang, Shumin Han, Errui Ding, and Di Huang. Student-teacher feature pyramid matching for anomaly detection. *arXiv preprint arXiv:2103.04257*, 2021. [1](#), [2](#)
- [54] Peter Welinder, Steve Branson, Takeshi Mita, Catherine Wah, Florian Schroff, Serge Belongie, and Pietro Perona. Caltech-ucsd birds 200. 2010. [4](#)
- [55] Peng Wu, Jing Liu, and Fang Shen. A deep one-class neural network for anomalous event detection in complex scenes. *IEEE transactions on neural networks and learning systems*, 31(7):2609–2622, 2019. [1](#), [2](#)
- [56] Guoyang Xie, Jinbao Wang, Jiaqi Liu, Jiayi Lyu, Yong Liu, Chengjie Wang, Feng Zheng, and Yaochu Jin. Im-ia-d: Industrial image anomaly detection benchmark in manufacturing. *IEEE Transactions on Cybernetics*, 2024. [2](#)
- [57] Xudong Yan, Huaidong Zhang, Xuemiao Xu, Xiaowei Hu, and Pheng-Ann Heng. Learning semantic context from normal samples for unsupervised anomaly detection. In *Proceedings of the AAAI Conference on Artificial Intelligence*, pages 3110–3118, 2021. [1](#), [2](#)
- [58] Jihun Yi and Sungroh Yoon. Patch svdd: Patch-level svdd for anomaly detection and segmentation. In *Proceedings of the Asian Conference on Computer Vision*, 2020. [1](#), [2](#)
- [59] Zhiyuan You, Lei Cui, Yujun Shen, Kai Yang, Xin Lu, Yu Zheng, and Xinyi Le. A unified model for multi-class anomaly detection. *Advances in Neural Information Processing Systems*, 35:4571–4584, 2022. [3](#)
- [60] Muhammad Zaigham Zaheer, Jin-ha Lee, Marcella Astrid, and Seung-Ik Lee. Old is gold: Redefining the adversarially learned one-class classifier training paradigm. In *Proceedings of the IEEE/CVF Conference on Computer Vision and Pattern Recognition*, pages 14183–14193, 2020. [1](#), [2](#)
- [61] Jerrold H Zar. Spearman rank correlation. *Encyclopedia of biostatistics*, 7, 2005. [6](#)
- [62] Vitjan Zavrtanik, Matej Kristan, and Danijel Skočaj. Draem—a discriminatively trained reconstruction embedding for surface anomaly detection. In *Proceedings of the IEEE/CVF international conference on computer vision*, pages 8330–8339, 2021. [2](#)
- [63] Vitjan Zavrtanik, Matej Kristan, and Danijel Skočaj. Reconstruction by inpainting for visual anomaly detection. *Pattern Recognition*, 112:107706, 2021. [1](#)
- [64] Vitjan Zavrtanik, Matej Kristan, and Danijel Skočaj. Dsr—a dual subspace re-projection network for surface anomaly detection. In *European conference on computer vision*, pages 539–554. Springer, 2022. [2](#)
- [65] Jiangning Zhang, Haoyang He, Zhenye Gan, Qingdong He, Yuxuan Cai, Zhucun Xue, Yabiao Wang, Chengjie Wang, Lei Xie, and Yong Liu. Ader: A comprehensive benchmark for multi-class visual anomaly detection. *arXiv preprint arXiv:2406.03262*, 2024. [2](#), [3](#)
- [66] Xuan Zhang, Shiyu Li, Xi Li, Ping Huang, Jiulong Shan, and Ting Chen. Destseg: Segmentation guided denoising student-teacher for anomaly detection. In *Proceedings of the IEEE/CVF Conference on Computer Vision and Pattern Recognition*, pages 3914–3923, 2023. [2](#)
- [67] Ximiao Zhang, Min Xu, and Xiuzhuang Zhou. Realnet: A feature selection network with realistic synthetic anomaly for anomaly detection. In *Proceedings of the IEEE/CVF Conference on Computer Vision and Pattern Recognition*, pages 16699–16708, 2024. [2](#)
- [68] Jiawen Zhu and Guansong Pang. Toward generalist anomaly detection via in-context residual learning with few-shot sample prompts. In *Proceedings of the IEEE/CVF Conference on Computer Vision and Pattern Recognition*, pages 17826–17836, 2024. [2](#), [5](#)
- [69] Yang Zou, Jongheon Jeong, Latha Pemula, Dongqing Zhang, and Onkar Dabeer. Spot-the-difference self-supervised pre-training for anomaly detection and segmentation. In *European Conference on Computer Vision*, pages 392–408. Springer, 2022. [1](#), [4](#)

A. Evaluation Metrics

A.1. AUROC metric

Area Under the Receiver Operating Characteristic (AUROC) [20] in the context of Multilevel Anomaly Detection (MAD) is defined as:

$$\text{AUROC} = \frac{\sum_{a=1}^n \sum_{x_i \in L_a} \sum_{x_j \in L_0} \mathbb{1}(f(x_i) > f(x_j))}{\sum_{a=1}^n |L_a| \cdot |L_0|},$$

where:

- n is the number of severity levels.
 - L_0 is the set of normal samples.
 - L_a (for $a = 1, 2, \dots, n$) are the sets of anomalous samples, grouped by severity level.
 - $f(x)$ is the anomaly score function.
 - $\mathbb{1}(\cdot)$ is the indicator function, equal to 1 if the condition inside is true and 0 otherwise.
 - $|L_a|$ and $|L_0|$ are the cardinalities (sizes) of the sets L_a and L_0 , respectively.
- AUROC achieves a perfect score of 1 if *all the anomaly scores of abnormal samples are greater than all the anomaly scores of normal samples*.

A.2. C-index metric

The C-index [51] is a generalization of the AUROC that can evaluate how well anomaly scores align with the severity levels. In the context of MAD, C-index is defined as:

$$C = \frac{\sum_{a=1}^n \sum_{b=0}^{a-1} \sum_{x_i \in L_a} \sum_{x_j \in L_b} \mathbb{1}(f(x_i) > f(x_j))}{\sum_{a=1}^n \sum_{b=0}^{a-1} |L_a| \cdot |L_b|},$$

A C-index of 1 corresponds to the best model prediction, achieved when *all samples from higher-severity levels are consistently assigned higher anomaly scores than samples from lower-severity levels or normal samples*. A C-index of 0.5 indicates a random prediction.

A.3. Kendall's Tau-b metric

In our paper, in addition to the C-index, we employ Kendall's Tau-b [25] for evaluating the consistency between anomaly scores and severity levels. Kendall's Tau-b, a stricter version of Kendall's Tau, is specifically chosen because it accounts for tied ranks, which is critical when samples within the same severity level are expected to have identical anomaly scores if we expect a perfect consistency (i.e., $\tau_b = 1$).

Suppose a pair of samples (x_i, x_j) is concordant if it follows the same order in terms of severity levels and anomaly scores. That is, if:

1. The severity level of sample x_i is greater than that of sample x_j , and the anomaly score of x_i is also greater than that of x_j or if
2. The severity level of sample x_i is less than that of sample x_j , and the anomaly score of x_i is also less than that of x_j .

The pair is discordant if it is in the reverse ordering for severity levels and anomaly score, or the values are arranged in opposite directions. That is, if:

1. The severity level of sample x_i is greater than that of sample x_j , but the anomaly score of x_i is less than that of x_j or if
2. The severity level of sample x_i is less than that of sample x_j , but the anomaly score of x_i is greater than that of x_j .

The two observations are tied if the severity level of sample x_i is equal that of x_j and/or the anomaly score of sample x_i is equal that of x_j .

Kendall's Tau-b is formulated as:

$$\tau_b = \frac{C - D}{\sqrt{(C + D + X_0)(C + D + Y_0)}},$$

where:

- C : The number of concordant pairs,
- D : The number of discordant pairs,
- X_0 : The number of pairs tied only on anomaly scores,
- Y_0 : The number of pairs tied only on severity levels.

Note that pairs where both the anomaly scores and severity levels are tied ($(XY)_0$) are excluded from both the numerator and denominator of Kendall’s Tau-b. This exclusion ensures that these pairs do not affect the metric’s calculation or penalize the performance.

The Kendall’s Tau-b ensures that tied pairs only on anomaly scores or only on severity levels are not ignored but instead reduce the overall Kendall’s Tau-b value to reflect the uncertainty caused by ties. Consequently, τ_b will be equal to 1.0 when *the ordering of anomaly scores perfectly corresponds to the ordering of severity levels, and all samples within the same severity level have identical anomaly scores*. This characteristic makes Kendall’s Tau-b particularly suitable in contexts where it is essential to ensure that a sample with a higher anomaly score always corresponds to a higher severity level. In contrast, the C-index can achieve a perfect score even when anomaly scores within the same severity level are not consistent, as it only considers pairwise comparisons across levels.

B. Prompts and Design Choices for MLLM-based baselines

B.1. Setup

For all experiments using MLLMs, we set the temperature to 0 to enable deterministic generation. The normal images are sourced from the training set and fixed for each subset.

B.2. Prompt design

We design prompts for MLLM-based baselines with the following key components, each carefully structured to guide the model’s performance effectively:

- **Context:** Provides detailed information about the normal reference images and the inference images for comparison. This section ensures the model understands the baseline for normalcy and the target images to evaluate.
- **Task Description:** Clearly defines the objectives of the multilevel anomaly detection task. This includes outlining the model’s role, such as identifying deviations between the reference and inference images and explaining the nature of potential anomalies.
- **Severity Levels Description:** Describes the various severity levels of anomalies to guide the model in interpreting and giving corresponding anomaly scores. The prompt specifies the characteristics of each level to standardize interpretation.
- **Format Guidelines:** Specifies the required structure and format for the model’s response to ensure clarity and consistency. The output format includes the following components:
 - Anomaly Score: A numerical value indicating the level of severity.
 - Reasoning: A concise yet comprehensive explanation of the detected anomaly, providing insights into the specific features or conditions that led to the classification.

Based on this design, five distinct prompts are provided, covering the following tasks: industrial inspection (MVTec-MAD and VisA-MAD), one-class novelty detection (MultiDogs-MAD), pulmonary imaging analysis (Covid19-MAD), diabetic retinopathy detection (DRD-MAD), and skin lesion detection (SkinLesion-MAD) (see text box below).

C. Zero-shot AD and Few-shot AD using MLLMs

Method	MultiDogs-MAD			MVTec-MAD			VisA-MAD			DRD-MAD			Covid19-MAD			SkinLesion-MAD			Average		
	AUC	Ken	C	AUC	Ken	C	AUC	Ken	C	AUC	Ken	C	AUC	Ken	C	AUC	Ken	C	AUC	Ken	C
RRD [49]	81.67	0.510	78.51	99.51	0.518	80.72	93.99	0.620	88.53	61.83	0.243	63.55	84.36	0.240	63.07	99.53	0.558	82.48	86.81	0.448	76.14
PNI [4]	77.20	0.413	73.11	99.32	0.487	78.91	96.07	0.622	88.64	62.50	0.285	65.94	87.96	0.241	63.12	100.0	0.455	76.51	87.17	0.417	74.37
GPT-4o (zero-shot)	98.67	0.942	98.44	82.16	0.525	75.11	68.70	0.422	68.22	50.25	0.044	50.29	50.95	0.064	50.63	61.33	0.180	55.77	68.68	0.363	66.41
Sonnet (zero-shot)	97.05	0.928	97.12	76.73	0.425	69.00	66.65	0.384	65.72	62.97	0.380	66.53	91.36	0.581	78.56	99.96	0.583	79.61	82.46	0.547	76.09
MMAD-4o	98.44	0.933	95.91	95.98	0.646	83.52	79.34	0.621	77.74	65.80	0.433	67.72	88.07	0.547	76.94	99.43	0.694	85.61	87.85	0.646	81.24
MMAD-Sonnet	97.89	0.936	97.34	90.02	0.557	77.33	76.24	0.561	74.86	65.02	0.403	69.30	92.35	0.601	80.54	99.82	0.610	79.23	86.89	0.611	79.77

Table 6. Multilevel AD performance comparison between zero-shot and few-shot learning on MLLM-based baselines and state-of-the-art conventional baselines across six datasets. The results are averaged across all subsets of each dataset. Higher AUROC (AUC) (%), Kendall’s Tau (Ken), and C-index (C) (%) values indicate better performance. Across most datasets, few-shot learning significantly outperforms zero-shot learning.

In addition to conducting experiments for few-shot settings on MLLMs (as reported in main paper), we also perform experiments under zero-shot settings. Specifically, in the zero-shot settings, we do not use normal images, aiming to evaluate

the model’s capability without reference images. The experimental results presented in Table 6 show that the performance of both Binary AD and Multilevel AD in zero-shot settings drops significantly compared to few-shot settings. This highlights the critical importance of using normal images as references in AD tasks.

D. Output Examples of MLLM-Based Baselines

This section provides examples of the output of MLLM-based baselines across datasets in Table 7, 8 and 9.

E. Number of samples across Severity Levels

We provide detailed number of samples across severity levels for each subset. The specifics are presented in Table 10, 11, 12, and 13, corresponding to the details of VisA-MAD, MVTec-MAD, MultiDogs-MAD, and the three medical datasets.

F. Full Results

We provide detailed results for each subset across severity levels on six datasets. The detailed results for each dataset in the MAD-Bench framework are provided in the corresponding tables: VisA-MAD results are in Tables 14 and 15, MVTec-MAD results are in Tables 16, 17, 18, MultiDogs-MAD results are in Table 19, DRD-MAD results are in Table 20, Covid19-MAD results are in Table 21, and SkinLesion-MAD results are detailed in Table 22.

The prompt for Industrial Inspection (MVTec-MAD and VisA-MAD)

System prompt:

You are a helpful assistant that responds in detecting anomalies on images in various context.

Instruction:

You are given four industrial inspection images:

Image 1, 2, 3: Belong to the non-defect category of {subset_name}.

Image 4: The inference image to be analyzed.

Your task is to determine an Anomaly Score for the inference image, reflecting the economic impact of the defect. A lower anomaly score suggests minimal economic impact, indicating that the item is likely usable or repairable, while a higher score indicates more severe impact, where the item may be unusable or costly to repair.

Use the following guidelines and ranges to assign the anomaly score:

- If the inference image is consistent with the non-defect category, assign a score of 0.
- If the inference image shows minor defects that are unlikely to impact functionality and may be easily repairable, assign a score between 1 and 30.
- If the inference image has defects suggesting moderate economic impact, where the item is still usable but may require repair, assign a score between 31 and 70.
- If the inference image displays severe defects with high economic impact, suggesting the item may be unusable or expensive to repair, assign a score between 71 and 100.

Output format:

Anomaly Score: [Score]

Reason: [Provide a brief explanation of why this score was assigned]

Please ensure the output strictly follows the format. You must answer the question even if you are not entirely certain about the answer.

The prompt for One-class Novelty Detection (MultiDogs-MAD)

System prompt:

You are a helpful assistant that responds in detecting anomalies on images in various context.

Instruction:

You are given four images:

Image 1, 2, 3: Belongs to the normal class {subset_name}.

Image 4: The inference image to be analyzed.

Your task is to determine an anomaly score for the inference image. This score should indicate how similar the inference image is to the class of the normal images. A lower anomaly score means the inference image is similar to the normal class, while a higher score indicates a greater deviation. Take into account the relationship between the class of the normal images and the class of the inference image. Carefully consider that there may be different levels of relationships between the normal class and the various abnormal classes. For example, some abnormal classes might be more closely related to the normal class (e.g., two different breeds of cats), while others might be completely different (e.g., a cat versus a completely unrelated object).

These relationships should reflect in the anomaly score:

- If the inference image belongs exactly to the same class as the normal images, assign a score of 0.
- If the inference image is similar but not identical to the normal class, assign a score between 1 and 50, with lower values indicating greater similarity.
- If the inference image belongs to an abnormal class but has some level of relationship to the normal class, assign a score between 51 and 75, considering the degree of similarity.
- If the inference image is completely unrelated to the normal class, assign a score between 76 and 100, with higher values indicating a greater dissimilarity.

Output format:

Anomaly Score: [Score]

Reason: [Provide a brief explanation of why this score was assigned]

Please ensure the output strictly follows the format. You must answer the question even you are not sure about the answer.

The prompt for DRD-MAD

System prompt:

You are a helpful assistant that responds in detecting anomalies on images in various context.

Instruction:

You are given four retinal images:

Image 1, 2, 3: Belongs to the normal retinal category (No DR).

Image 4: The inference image to be analyzed.

Your task is to determine an Anomaly Score for the inference image on a scale from 0 to 100, reflecting the extent of diabetic retinopathy (DR). A lower anomaly score suggests minimal or no DR, while a higher score indicates more severe stages of DR.

Use the following guidelines to assign the Anomaly Score:

- If the inference image shows no signs of diabetic retinopathy, assign a score of 0.
- If the inference image shows mild signs of diabetic retinopathy, assign an anomaly score between 1 and 25.
- If the inference image has characteristics suggesting moderate diabetic retinopathy, assign an anomaly score between 26 and 50.
- If the inference image displays severe diabetic retinopathy, assign an anomaly score between 51 and 75.
- If the inference image reveals advanced proliferative diabetic retinopathy, assign an anomaly score between 76 and 100.

Output format:

Anomaly Score: [Score]

Reason: [Provide a brief explanation of why this score was assigned]

Please ensure the output strictly follows the format. You must answer the question even if you are not entirely certain about the answer.

The prompt for Covid19-MAD

System prompt:

You are a helpful assistant that responds in detecting anomalies on images in various context.

Instruction:

You are given four lung scan images:

Image 1, 2, 3: Belongs to the normal lung category.

Image 4: The inference image to be analyzed.

Your task is to determine an anomaly score for the inference image on a scale from 0 to 100, reflecting the extent of lung damage. A lower anomaly score suggests minimal or no lung damage, while a higher score indicates more severe lung damage.

Use the following guidelines to assign the anomaly score:

- If the inference image is consistent with a normal lung, assign a score of 0.
- If the inference image shows very mild lung damage, such as isolated ground-glass opacities, assign a score between 1 and 15.
- If the inference image shows mild lung damage, with limited areas of ground-glass opacities, assign a score between 16 and 30.
- If the inference image has moderate lung damage, such as more widespread ground-glass opacities, assign a score between 31 and 50.
- If the inference image displays moderately severe lung damage, including partial lung consolidation, assign a score between 51 and 70.
- If the inference image shows severe lung damage, such as extensive consolidation in multiple lung regions, assign a score between 71 and 85.
- If the inference image reveals extreme lung damage, affecting more than 85 percent of the lungs, assign a score between 86 and 100.

Output format:

Anomaly Score: [Score]

Reason: [Provide a brief explanation of why this score was assigned]

Please ensure the output strictly follows the format. You must answer the question even if you are not entirely certain about the answer.

The prompt for SkinLesion-MAD

System prompt:

You are a helpful assistant that responds in detecting anomalies on images in various context.

Instruction:

You are given four dermoscopic images:

Image 1, 2, 3: Belong to the normal skin category.

Image 4: The inference image to be analyzed.

Your task is to determine an anomaly score for the inference image, reflecting its potential danger level in comparison to normal skin. A lower anomaly score suggests that the lesion is benign, while a higher score indicates a more dangerous lesion type, such as precancerous or cancerous.

Use the following guidelines and ranges to assign the anomaly score:

- If the inference image is consistent with normal skin, assign a score of 0.
- If the inference image appears benign but shows minor atypical features, such as a mole (nevus) with slightly irregular borders, assign a score between 1 and 30 to indicate a benign lesion.
- If the inference image has characteristics suggesting it could be precancerous, assign a score between 31 and 70.
- If the inference image displays features strongly associated with malignancy, assign a score between 71 and 100, indicating a high risk for cancer.

Output format:

Anomaly Score: [Score]

Reason: [Provide a brief explanation of why this score was assigned]

Please ensure the output strictly follows the format. You must answer the question even if you are not entirely certain about the answer.



<p>Normal Image</p> 	<p>Subset: Hazelnut in MVTec-MAD.</p>	<p>Severity Level (GT): 3/3. The hazelnut has a large crack, indicating a high economic impact.</p>
<p>Inference Image</p> 		
<p>Output from MMAD-4o</p>	<p>Anomaly Score: 71. Reason: The inference image shows a significant hole in the hazelnut, which is a severe defect. This type of damage likely renders the nut unusable or costly to repair, indicating a high economic impact.</p>	
<p>Output from MMAD-Sonnet</p>	<p>Anomaly Score: 85. Reason: The inference image shows a significant defect in the form of a hole or perforation in the hazelnut shell, along with what appears to be some discoloration around the damaged area. This type of damage likely indicates pest infestation or severe physical damage, which makes the hazelnut unsuitable for commercial sale or consumption. Such defects have a high economic impact as the product must be discarded due to food safety concerns and quality standards. Unlike minor surface blemishes, this type of structural damage cannot be repaired or salvaged, hence the high anomaly score.</p>	

Table 7. The output of MLLM-based baselines on a sample in MVTec-MAD dataset.


<p>Normal Image</p> 	<p>Subset Name: Golden Retriever in MultiDogs-MAD (Normal images). The inference image depicts a dog of a different breed than the Golden Retriever.</p>	<p>Severity Level (GT): 1/4. The dog is of a different breed than the Golden Retriever but is still a dog.</p>
<p>Inference Image</p> 		
<p>Output from MMAD-4o</p>	<p>Anomaly Score: 51. Reason: The inference image depicts a dog that is not a golden retriever but is still a dog, indicating some level of relationship to the normal class. This results in a moderate anomaly score reflecting the similarity.</p>	
<p>Output from MMAD-Sonnet</p>	<p>Anomaly Score: 35. Reason: The inference image shows a Curly-Coated Retriever, which is different from but related to Golden Retrievers shown in the normal images. While it's not the same breed, it belongs to the same retriever family of dogs, sharing similar characteristics like body structure, general size, and purpose (retrieving dogs). The main differences are the black color and curly coat texture, as opposed to the golden straight coat of Golden Retrievers. The score of 35 reflects that while this is a different breed, it's still closely related to the normal class, being from the same retriever family, showing similar facial features, body structure, and behavioral characteristics typical of retriever breeds.</p>	

Table 8. The output of MLLM-based baselines on a sample in MultiDogs-MAD dataset.

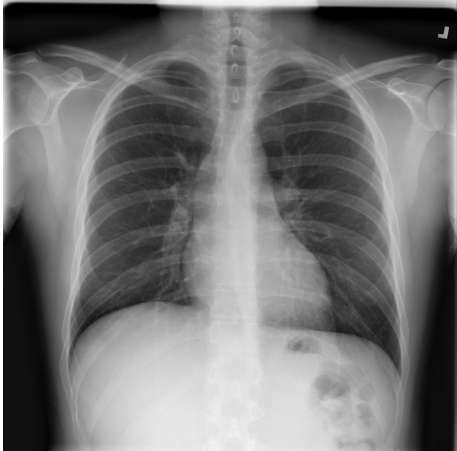
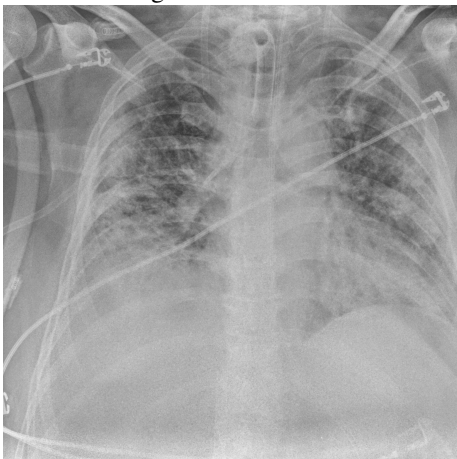
<p>Normal Image</p> 	<p>Dataset Name: Covid19-MAD</p>	<p>Severity Level (GT): 6/6. The inference image shows extreme lung damage, affecting more than 85% of the lung.</p>
<p>Inference Image</p> 		
<p>Output from MMAD-4o</p>	<p>Anomaly Score: 75. Reason: The inference image shows extensive consolidation in multiple lung regions, indicating severe lung damage. This is more pronounced compared to the normal lung images provided.</p>	
<p>Output from MMAD-Sonnet</p>	<p>Anomaly Score: 75. Reason: The inference image shows significant abnormalities compared to the normal lung images. There are extensive bilateral ground-glass opacities and consolidation patterns throughout both lung fields, particularly in the mid and lower zones. The lung fields appear much hazier and whiter compared to the clear, dark lung fields seen in the normal images. The presence of medical equipment (tubes/lines) also suggests a severe clinical condition. The extent and distribution of the abnormalities affect approximately 75-80% of the visible lung fields, placing this case in the severe category (71-85 range) of lung damage. While severe, it's not in the extreme category as there are still some areas of relatively preserved lung tissue visible.</p>	

Table 9. The output of MLLM-based baselines on a sample in Covid19-MAD dataset.

Level	Capsules	Chewinggum	Fryum	Macaroni1	Macaroni2	PCB1	PCB2	PCB3	Pipe_Fryum
Level 0 (training)	542	453	450	900	900	904	901	905	450
Level 0 (test)	60	50	50	100	100	100	100	101	50
Level 1	45	40	6	16	16	14	14	20	39
Level 2	20	8	35	12	9	66	67	60	15
Level 3	20	23	59	35	35	20	19	20	25
Total	687	574	600	1063	1060	1104	1101	1106	579

Table 10. Number of samples of the VisA-MAD dataset across levels.

Level	Carpet	Grid	Leather	Tile	Wood	Bottle	Cable	Capsule	Hazelnut	Metal_nut	Pill	Screw	Transistor	Zipper
Level 0 (training)	280	264	245	230	247	209	224	219	391	220	267	320	213	240
Level 0 (test)	28	21	32	33	19	20	58	23	40	22	26	41	60	32
Level 1	17	33	38	36	18	21	23	45	17	22	43	25	10	33
Level 2	19	12	17	31	31	22	22	20	17	23	26	24	10	70
Level 3	34	12	37	17	11	20	11	44	36	25	17	24	20	16
Total	378	342	369	347	326	292	338	351	501	312	379	434	313	391

Table 11. Number of samples of MVTec-MAD dataset across levels.

Level	Bichon Frise	Chinese Rural Dog	Golden Retriever	Labrador Retriever	Teddy
Level 0 (training)	500	500	500	500	500
Level 0 (test)	500	500	500	500	500
Level 1	500	500	500	500	500
Level 2	500	500	500	500	500
Level 3	500	500	500	500	500
Level 4	500	500	500	500	500
Total	2500	2500	2500	2500	2500

Table 12. Number of samples of MultiDogs-MAD datasets across levels.

Level	Covid-MAD	DRD-MAD	SkinLesion-MAD
Leve 0 (training)	703	1000	500
Level 0 (test)	81	700	500
Level 1	96	700	642
Level 2	60	700	327
Level 3	62	700	500
Level 4	90	700	None
Level 5	135	None	None
Level 6	137	None	None
Total	1364	4500	2469

Table 13. Number of samples of three medical datasets across levels.

Method	Binary AD performance				MAD performance		Binary AD performance				MAD performance	
	Level 1	Level 2	Level 3	Whole	Ken	C	Level 1	Level 2	Level 3	Whole	Ken	C
	capsules						chewinggum					
Skip-GAN [2]	63.11	79.58	71.08	68.86	0.286	67.12	82.55	92.00	96.00	87.97	0.560	83.84
RD4AD [12]	85.26	98.33	98.50	91.45	0.701	91.93	95.30	100.0	100.0	97.35	0.736	94.45
PatchCore [39]	67.26	85.42	94.75	78.00	0.479	78.66	96.65	100.0	100.0	98.11	0.727	93.93
CFLOW-AD [18]	61.41	94.00	87.58	75.24	0.416	74.89	98.00	100.0	100.0	98.87	0.714	93.14
RRD [49]	86.37	99.58	99.50	92.57	0.688	91.12	97.50	100.0	100.0	98.59	0.745	94.99
OCR-GAN [31]	89.48	84.50	80.08	86.10	0.310	68.51	91.80	92.75	94.96	92.93	0.572	84.56
PNI [4]	82.19	94.92	98.58	89.04	0.617	86.88	98.00	100.0	100.0	98.87	0.728	93.97
SPR [46]	67.19	85.08	74.42	73.10	0.311	68.60	35.95	31.75	30.26	33.63	0.213	37.13
IGD [9]	56.22	66.08	68.17	61.35	0.183	60.95	88.90	100.0	98.87	93.38	0.626	87.82
AE4AD [7]	70.83	80.75	67.26	71.27	0.291	67.38	76.09	65.75	68.55	70.68	0.264	65.96
MMAD-4o	70.00	85.00	100.0	80.59	0.726	82.23	93.75	100.0	100.0	96.48	0.832	93.32
MMAD-4o-mini	80.00	80.00	97.50	84.12	0.665	80.40	92.75	96.25	99.13	95.21	0.756	89.79
MMAD-Sonnet	52.22	75.00	82.50	64.71	0.537	67.75	87.32	97.75	99.61	92.48	0.756	89.44
MMAD-Haiku	50.00	50.00	50.00	50.00	nan	50.00	83.75	100.0	100.0	90.85	0.748	85.89
	fryum						macaroni1					
Skip-GAN [2]	49.00	92.91	100.0	94.46	0.680	91.15	96.06	90.00	100.0	97.10	0.682	95.34
RD4AD [12]	73.33	90.51	99.97	95.06	0.746	95.15	97.38	97.33	97.63	97.51	0.664	94.11
PatchCore [39]	78.67	92.63	100.0	96.14	0.758	95.86	97.19	98.58	96.66	97.16	0.628	91.74
CFLOW-AD [18]	60.67	83.77	96.98	90.18	0.632	88.27	87.38	91.42	77.14	82.46	0.397	76.38
RRD [49]	77.33	86.29	99.86	93.76	0.731	94.21	91.31	94.75	94.23	93.59	0.597	89.69
OCR-GAN [31]	94.00	86.57	88.61	88.22	0.454	77.45	98.19	98.75	93.37	95.62	0.633	92.04
PNI [4]	85.00	97.89	100.0	98.36	0.759	95.92	97.56	99.42	96.46	97.30	0.605	90.22
SPR [46]	60.00	62.97	75.73	70.32	0.305	68.44	52.50	47.50	71.34	62.02	0.193	62.81
IGD [9]	82.33	77.49	90.81	85.64	0.516	81.24	80.50	78.25	65.43	71.70	0.241	66.03
AE4AD [7]	87.69	63.37	85.67	79.06	0.436	76.39	64.86	79.58	82.06	72.03	0.248	66.50
MMAD-4o	50.00	77.14	96.61	87.00	0.745	87.86	52.62	57.83	82.40	70.16	0.584	70.80
MMAD-4o-mini	54.33	75.26	94.68	85.46	0.688	85.12	49.62	63.17	73.31	65.37	0.423	65.87
MMAD-Sonnet	50.00	70.00	89.83	80.50	0.665	81.37	56.25	58.33	82.86	71.43	0.605	71.92
MMAD-Haiku	50.00	55.71	67.80	62.50	0.382	62.64	49.00	49.00	69.20	60.22	0.396	61.24
	macaroni2						pcb1					
Skip-GAN [2]	45.00	53.67	50.46	49.48	0.000	49.99	82.00	87.24	90.05	87.07	0.513	82.35
RD4AD [12]	91.81	80.56	87.40	87.55	0.479	82.21	97.71	97.02	94.20	96.55	0.604	88.08
PatchCore [39]	91.56	77.33	69.77	76.72	0.300	70.21	98.50	98.61	96.70	98.21	0.644	90.57
CFLOW-AD [18]	58.50	46.78	50.94	52.33	0.021	51.39	94.86	93.70	99.05	94.93	0.646	90.68
RRD [49]	92.56	71.67	85.69	85.42	0.447	80.08	94.29	95.50	94.70	95.17	0.612	88.54
OCR-GAN [31]	94.00	90.56	93.00	92.90	0.545	86.66	93.93	93.56	93.65	93.63	0.569	85.87
PNI [4]	98.19	79.56	77.26	83.18	0.364	74.51	99.79	99.61	98.90	99.49	0.656	91.36
SPR [46]	55.56	58.33	53.80	54.95	0.059	53.97	30.14	54.29	41.60	48.37	0.014	49.14
IGD [9]	66.75	70.00	62.46	64.73	0.170	61.43	89.71	90.20	98.85	91.86	0.618	88.92
AE4AD [7]	75.26	73.22	79.25	76.02	0.320	71.53	84.82	95.40	90.64	87.75	0.522	82.87
MMAD-4o	53.12	50.00	61.43	57.50	0.342	57.52	58.82	81.01	71.40	75.98	0.536	73.38
MMAD-4o-mini	38.50	60.61	60.13	54.43	0.108	55.93	60.86	75.00	70.10	72.04	0.448	69.26
MMAD-Sonnet	51.28	47.78	60.00	55.84	0.120	56.20	53.36	76.83	90.95	76.36	0.585	76.58
MMAD-Haiku	48.00	53.56	50.86	50.50	0.033	50.65	49.50	51.03	57.07	52.02	0.166	52.54

Table 14. Full results on VisA-MAD (Part I)

Method	Binary AD performance			MAD performance			Binary AD performance			MAD performance		
	Level 1	Level 2	Level 3	Whole	Ken	C	Level 1	Level 2	Level 3	Whole	Ken	C
	pcb2						pcb3					
Skip-GAN [2]	75.57	99.37	100.0	96.16	0.703	94.41	71.68	93.71	94.50	89.47	0.576	85.96
RD4AD [12]	98.93	97.67	90.00	96.39	0.555	85.04	96.68	98.00	90.10	96.16	0.570	85.57
PatchCore [39]	100.0	98.46	91.84	97.42	0.578	86.48	97.82	99.08	97.08	98.43	0.599	87.38
CFLOW-AD [18]	92.43	89.75	86.47	89.50	0.516	82.57	85.20	84.85	85.94	85.14	0.458	78.61
RRD [49]	98.36	93.04	78.95	91.11	0.484	80.56	96.73	96.40	94.46	96.08	0.590	86.82
OCR-GAN [31]	95.71	96.85	98.79	97.06	0.666	92.07	82.97	85.59	88.76	85.70	0.504	81.48
PNI [4]	100.0	99.75	95.84	99.04	0.596	87.66	99.36	99.79	99.01	99.54	0.609	88.03
SPR [46]	48.29	58.40	47.58	54.93	0.058	53.64	51.78	63.20	68.66	62.01	0.184	61.48
IGD [9]	71.93	83.16	93.63	83.58	0.486	80.70	71.88	76.65	88.47	78.06	0.414	75.81
AE4AD [7]	96.66	99.53	90.29	96.31	0.683	93.10	74.26	90.54	71.73	77.01	0.407	75.39
MMAD-4o	9.89	75.96	71.84	75.72	0.490	71.94	67.50	78.33	62.50	73.00	0.475	68.62
MMAD-4o-mini	70.00	69.93	62.68	68.56	0.290	64.06	63.24	80.09	59.95	72.69	0.367	67.36
MMAD-Sonnet	77.71	81.66	73.16	79.49	0.556	74.74	67.50	72.50	67.50	70.50	0.450	66.78
MMAD-Haiku	62.89	65.05	51.21	62.12	0.257	58.36	51.98	56.20	49.50	54.02	0.148	52.87
	pipe_fryum						mean					
Skip-GAN [2]	63.69	73.07	88.00	73.16	0.380	72.49	69.85	84.62	87.79	82.64	0.487	80.29
RD4AD [12]	98.41	100.0	99.84	99.16	0.701	91.54	92.76	95.49	95.29	95.24	0.640	89.79
PatchCore [39]	99.38	100.0	100.0	99.70	0.708	91.91	91.89	94.46	94.09	93.32	0.602	87.42
CFLOW-AD [18]	95.38	100.0	97.92	97.06	0.640	87.92	81.54	87.14	86.89	85.08	0.493	80.43
RRD [49]	99.38	99.87	99.92	99.65	0.688	90.72	92.65	93.01	94.15	93.99	0.620	88.53
OCR-GAN [31]	80.97	97.60	94.32	88.35	0.483	78.61	91.23	91.86	91.73	91.17	0.526	83.03
PNI [4]	99.74	100.0	99.76	99.80	0.662	89.21	95.54	96.77	96.20	96.07	0.622	88.64
SPR [46]	49.49	46.53	37.44	45.11	0.097	44.23	50.10	56.45	55.65	56.05	0.087	55.49
IGD [9]	75.64	90.40	92.40	83.75	0.516	80.56	75.98	81.36	84.34	79.34	0.419	75.94
AE4AD [7]	62.40	63.60	45.79	54.58	0.115	56.79	76.99	79.08	75.69	76.08	0.365	72.88
MMAD-4o	96.15	98.47	99.56	97.67	0.857	94.03	61.32	78.19	82.86	79.34	0.621	77.74
MMAD-4o-mini	85.18	87.87	98.96	90.05	0.756	88.76	66.05	76.46	79.60	76.44	0.500	74.06
MMAD-Sonnet	92.00	96.60	98.36	94.89	0.775	88.97	65.29	75.16	82.75	76.24	0.561	74.86
MMAD-Haiku	69.23	93.33	70.00	74.05	0.479	69.69	57.15	63.76	62.85	61.81	0.326	60.43

Table 15. Full results on VisA-MAD (Part II)

Method	Binary AD performance			MAD performance			Binary AD performance			MAD performance		
	Level 1	Level 2	Level 3	Whole	Ken	C	Level 1	Level 2	Level 3	Whole	Ken	C
carpet												
Skip-GAN [2]	29.20	47.18	70.90	54.34	0.243	64.13	72.87	90.08	54.37	72.60	0.150	58.88
RD4AD [12]	100.0	100.0	100.0	100.0	0.587	84.17	100.0	100.0	100.0	100.0	0.616	86.54
PatchCore [39]	97.06	100.0	100.0	99.29	0.663	88.59	96.54	100.0	100.0	97.99	0.659	89.08
CFLOW-AD [18]	100.0	93.61	100.0	98.27	0.446	75.93	90.91	94.84	98.81	93.40	0.482	78.62
RRD [49]	100.0	100.0	100.0	100.0	0.582	83.89	100.0	100.0	100.0	100.0	0.659	89.08
OCR-GAN [31]	94.12	100.0	100.0	98.57	0.286	66.67	97.40	100.0	100.0	98.50	0.550	82.61
PNI [4]	100.0	99.44	100.0	99.85	0.616	85.83	97.40	100.0	100.0	98.50	0.579	84.34
SPR [46]	83.40	100.0	95.06	93.57	0.443	75.79	100.0	100.0	100.0	100.0	0.342	70.28
IGD [9]	64.29	73.87	86.34	77.60	0.383	72.28	68.25	72.62	59.52	67.34	0.127	57.52
AE4AD [7]	5.46	78.20	60.50	51.94	0.171	59.94	66.81	82.54	69.84	70.76	0.268	65.87
MMAD-4o	100.0	100.0	100.0	100.0	0.811	92.10	98.48	100.0	100.0	99.12	0.683	86.80
MMAD-4o-mini	100.0	100.0	100.0	100.0	0.752	87.62	94.23	98.81	100.0	96.41	0.755	89.52
MMAD-Sonnet	100.0	100.0	98.53	99.29	0.744	86.93	96.97	95.83	100.0	97.37	0.728	86.97
MMAD-Haiku	91.18	89.47	94.12	92.14	0.579	78.81	80.30	83.33	100.0	85.09	0.552	75.55
tile												
Skip-GAN [2]	47.70	16.36	10.05	26.77	0.437	24.55	76.68	74.68	85.92	77.81	0.249	64.45
RD4AD [12]	100.0	100.0	100.0	100.0	0.473	77.55	100.0	98.44	100.0	99.42	0.422	74.52
PatchCore [39]	100.0	100.0	100.0	100.0	0.456	76.55	100.0	96.97	100.0	98.88	0.445	75.85
CFLOW-AD [18]	99.84	100.0	100.0	99.93	0.412	73.96	100.0	98.34	100.0	99.39	0.391	72.73
RRD [49]	100.0	100.0	100.0	100.0	0.536	81.21	100.0	99.22	100.0	99.71	0.440	75.57
OCR-GAN [31]	100.0	100.0	100.0	100.0	0.654	88.05	99.49	96.19	96.43	97.66	0.247	64.35
PNI [4]	99.42	100.0	100.0	99.76	0.464	77.01	100.0	99.61	100.0	99.86	0.461	76.77
SPR [46]	99.84	100.0	99.92	99.90	0.425	74.72	99.66	100.0	100.0	99.86	0.398	73.11
IGD [9]	88.49	97.24	87.58	89.74	0.363	71.11	100.0	93.45	100.0	97.58	0.469	77.26
AE4AD [7]	67.68	97.43	73.90	75.68	0.290	66.90	51.52	54.25	57.22	53.68	0.055	53.19
MMAD-4o	99.05	100.0	100.0	99.61	0.782	91.27	100.0	100.0	100.0	100.0	0.623	82.74
MMAD-4o-mini	98.89	100.0	100.0	99.54	0.750	86.30	100.0	87.10	100.0	95.24	0.483	75.17
MMAD-Sonnet	100.0	100.0	100.0	100.0	0.658	82.28	100.0	95.01	100.0	98.16	0.544	78.06
MMAD-Haiku	98.48	99.91	98.44	98.73	0.578	78.38	94.44	74.19	100.0	88.10	0.477	73.71
wood												
Skip-GAN [2]	83.92	95.76	89.00	90.96	0.451	76.49	60.00	58.41	42.00	53.73	0.078	45.55
RD4AD [12]	100.0	98.47	100.0	99.21	0.548	82.16	99.76	100.0	100.0	99.92	0.602	84.55
PatchCore [39]	100.0	98.13	100.0	99.04	0.491	78.81	100.0	100.0	100.0	100.0	0.580	83.27
CFLOW-AD [18]	100.0	97.28	100.0	98.60	0.474	77.78	100.0	100.0	100.0	100.0	0.526	80.21
RRD [49]	100.0	98.64	100.0	99.30	0.535	81.40	100.0	100.0	100.0	100.0	0.567	82.57
OCR-GAN [31]	87.43	100.0	100.0	96.23	0.688	90.34	97.14	100.0	100.0	99.05	0.458	76.30
PNI [4]	100.0	98.47	100.0	99.21	0.438	75.68	100.0	100.0	100.0	100.0	0.609	84.93
SPR [46]	99.84	100.0	99.92	99.90	0.425	74.72	99.66	100.0	100.0	99.86	0.398	73.11
IGD [9]	100.0	95.93	100.0	97.89	0.461	77.02	98.81	99.77	100.0	99.52	0.453	75.99
AE4AD [7]	85.67	86.08	82.78	85.35	0.372	71.84	95.48	93.18	100.0	96.11	0.441	75.33
MMAD-4o	94.88	95.93	98.33	96.05	0.596	81.31	100.0	100.0	100.0	100.0	0.721	87.66
MMAD-4o-mini	95.18	97.45	99.28	97.11	0.628	83.57	98.57	100.0	100.0	99.52	0.731	89.78
MMAD-Sonnet	100.0	99.49	100.0	99.74	0.580	79.73	86.67	99.55	100.0	95.40	0.639	80.89
MMAD-Haiku	96.78	95.67	97.13	96.27	0.579	75.57	76.19	90.91	92.50	86.51	0.607	79.45
bottle												
Skip-GAN [2]	47.75	32.52	24.45	37.19	0.219	36.55	44.83	94.57	50.59	56.28	0.078	54.56
RD4AD [12]	95.73	99.14	99.22	97.75	0.568	84.98	95.85	100.0	98.32	97.61	0.543	81.89
PatchCore [39]	99.78	99.37	100.0	99.66	0.635	89.10	96.14	100.0	98.81	97.93	0.480	78.17
CFLOW-AD [18]	94.60	95.61	99.69	96.00	0.579	85.62	92.08	99.78	97.73	95.77	0.437	75.65
RRD [49]	99.55	100.0	100.0	99.82	0.591	86.37	98.26	100.0	99.21	98.96	0.545	82.00
OCR-GAN [31]	78.94	94.12	88.87	86.85	0.524	82.28	90.05	100.0	95.95	94.26	0.270	65.87
PNI [4]	98.35	98.90	100.0	98.89	0.676	91.60	99.42	100.0	99.31	99.48	0.360	71.17
SPR [46]	97.90	85.97	99.53	93.53	0.527	82.47	95.94	100.0	97.83	97.45	0.581	84.12
IGD [9]	90.93	93.18	98.28	93.26	0.572	85.22	80.19	99.78	86.46	86.32	0.347	70.40
AE4AD [7]	64.77	88.56	87.77	78.63	0.435	76.75	62.80	99.35	63.44	69.76	0.150	58.78
MMAD-4o	99.06	99.96	100.0	99.60	0.835	93.28	91.88	94.67	96.44	94.24	0.422	72.43
MMAD-4o-mini	93.85	94.59	94.20	94.21	0.647	84.93	88.02	99.57	95.16	93.02	0.492	74.01
MMAD-Sonnet	94.19	97.02	98.98	96.24	0.805	88.66	82.85	81.52	86.41	84.04	0.356	67.59
MMAD-Haiku	60.87	75.00	81.82	70.54	0.519	68.75	61.11	50.00	70.45	62.84	0.269	59.59
capsule												

Table 16. Full results on MVTec-MAD (Part I)

Method	Binary AD performance					MAD performance		Binary AD performance					MAD performance	
	Level 1	Level 2	Level 3	Whole	Ken	C	Level 1	Level 2	Level 3	Whole	Ken	C		
	hazelnut						metal_nut							
Skip-GAN [2]	100.0	69.56	77.57	81.07	0.218	62.83	43.39	26.09	57.27	42.66	0.084	54.84		
RD4AD [12]	100.0	100.0	100.0	100.0	0.560	82.98	100.0	100.0	100.0	100.0	0.469	76.92		
PatchCore [39]	100.0	100.0	100.0	100.0	0.504	79.71	100.0	99.60	100.0	99.87	0.455	76.13		
CFLOW-AD [18]	100.0	100.0	100.0	100.0	0.611	86.02	98.76	90.91	99.64	96.49	0.430	74.68		
RRD [49]	100.0	100.0	100.0	100.0	0.563	83.19	100.0	100.0	100.0	100.0	0.504	78.93		
OCR-GAN [31]	99.85	90.15	99.10	97.11	0.482	78.44	73.55	100.0	99.09	91.36	0.212	62.16		
PNI [4]	100.0	100.0	100.0	100.0	0.448	76.42	100.0	100.0	100.0	100.0	0.431	74.74		
SPR [46]	100.0	94.26	100.0	98.61	0.466	77.49	99.59	86.36	100.0	95.39	0.388	72.31		
IGD [9]	93.38	95.29	98.40	96.43	0.636	87.48	79.55	94.86	75.45	83.12	0.222	62.72		
AE4AD [7]	99.26	68.82	85.28	84.68	0.319	68.82	48.55	45.45	49.64	47.92	0.026	48.53		
MMAD-4o	99.26	98.38	100.0	99.43	0.834	94.05	100.0	100.0	100.0	100.0	0.636	82.89		
MMAD-4o-mini	85.07	84.19	98.58	91.80	0.713	88.72	89.15	99.01	91.73	93.31	0.636	82.73		
MMAD-Sonnet	94.41	97.57	98.75	97.41	0.825	91.27	95.45	80.43	78.00	84.29	0.363	67.19		
MMAD-Haiku	80.15	72.57	92.64	84.73	0.545	79.32	88.64	63.04	56.00	68.57	0.044	48.28		
	pill						screw							
Skip-GAN [2]	66.55	80.33	96.83	76.70	0.512	80.01	65.85	0.00	0.00	22.55	0.496	21.20		
RD4AD [12]	100.0	92.46	100.0	97.72	0.438	75.64	99.41	99.59	95.93	98.33	0.286	66.60		
PatchCore [39]	98.03	90.24	99.55	95.97	0.483	78.29	99.90	99.59	98.98	99.50	0.318	68.48		
CFLOW-AD [18]	94.19	85.36	96.83	92.04	0.457	76.78	97.07	97.15	95.02	96.42	0.439	75.51		
RRD [49]	100.0	96.15	100.0	98.84	0.440	75.77	99.61	100.0	98.78	99.47	0.286	66.60		
OCR-GAN [31]	97.50	100.0	98.19	98.39	0.185	60.86	84.68	50.61	74.29	70.06	0.122	57.10		
PNI [4]	98.39	88.17	99.77	95.57	0.421	74.69	100.0	100.0	98.48	99.50	0.322	68.71		
SPR [46]	92.49	89.94	100.0	93.20	0.495	78.97	98.73	98.98	98.88	98.86	0.420	74.40		
IGD [9]	89.18	77.37	93.67	86.49	0.407	73.82	75.32	72.76	60.47	69.60	0.128	57.43		
AE4AD [7]	67.62	81.07	96.61	77.42	0.476	77.91	27.90	40.96	61.38	43.20	0.055	53.20		
MMAD-4o	97.67	84.62	100.0	94.19	0.498	75.68	96.00	77.08	81.25	84.93	0.480	72.44		
MMAD-4o-mini	96.87	88.61	100.0	94.99	0.603	80.87	82.59	80.39	91.41	84.76	0.574	78.97		
MMAD-Sonnet	75.22	59.69	87.44	72.94	0.307	63.63	72.39	65.75	74.44	70.88	0.323	65.36		
MMAD-Haiku	60.87	50.00	59.73	57.36	0.054	51.63	54.00	52.08	52.08	52.74	0.080	51.22		
	transistor						zipper							
Skip-GAN [2]	86.33	73.00	52.08	65.88	0.137	58.97	70.83	37.54	60.74	49.89	0.102	43.87		
RD4AD [12]	88.17	98.67	99.50	96.46	0.549	85.83	98.30	98.26	99.61	98.45	0.392	73.65		
PatchCore [39]	100.0	100.0	100.0	100.0	0.625	90.83	99.15	99.51	100.0	99.47	0.368	72.20		
CFLOW-AD [18]	100.0	96.33	84.92	91.54	0.437	78.52	92.71	98.79	99.61	97.22	0.399	74.11		
RRD [49]	95.83	99.67	99.17	98.46	0.570	87.24	97.73	98.66	99.80	98.56	0.434	76.19		
OCR-GAN [31]	100.0	99.50	96.50	98.12	0.519	83.93	94.32	96.16	93.16	95.25	0.424	75.62		
PNI [4]	100.0	100.0	100.0	100.0	0.573	87.41	99.62	99.87	100.0	99.82	0.421	75.41		
SPR [46]	100.0	100.0	97.00	98.50	0.524	84.21	99.81	100.0	100.0	99.95	0.484	79.24		
IGD [9]	100.0	88.83	86.67	90.54	0.426	77.83	87.03	92.81	98.05	91.91	0.383	73.11		
AE4AD [7]	100.0	85.50	72.17	82.46	0.317	70.72	81.34	82.37	90.04	83.11	0.297	67.91		
MMAD-4o	72.92	72.75	96.33	84.58	0.636	80.84	98.48	87.86	96.88	92.02	0.485	75.79		
MMAD-4o-mini	67.67	65.67	87.00	76.83	0.478	75.16	98.48	87.14	96.88	91.60	0.358	69.09		
MMAD-Sonnet	93.83	82.75	87.83	88.06	0.621	79.69	84.85	69.29	90.62	76.47	0.303	64.35		
MMAD-Haiku	61.00	50.00	71.25	63.38	0.336	62.90	69.70	52.14	62.50	58.40	0.010	49.70		

Table 17. Full results on MVTec-MAD (Part II)

Method	Binary AD performance				MAD performance	
	Level 1	Level 2	Level 3	Whole	Ken	C
	mean					
Skip-GAN [2]	63.99	56.86	55.13	57.75	0.057	53.35
RD4AD [12]	98.37	98.93	99.47	98.92	0.504	79.86
PatchCore [39]	99.04	98.82	99.81	99.11	0.511	80.36
CFLOW-AD [18]	97.15	96.29	98.02	96.79	0.466	77.58
RRD [49]	99.36	99.45	99.78	99.51	0.518	80.72
OCR-GAN [31]	92.46	94.77	95.83	94.39	0.402	73.90
PNI [4]	99.47	98.89	99.83	99.32	0.487	78.91
SPR [46]	97.63	96.82	99.15	97.76	0.451	76.78
IGD [9]	86.82	89.13	87.92	87.67	0.384	72.78
AE4AD [7]	66.06	77.41	75.04	71.48	0.259	65.41
MMAD-4o	96.26	93.66	97.80	95.98	0.646	83.52
MMAD-4o-mini	92.04	91.61	96.73	93.45	0.614	81.89
MMAD-Sonnet	91.20	87.42	92.93	90.02	0.557	77.33
MMAD-Haiku	76.69	71.31	80.62	76.10	0.366	66.63

Table 18. Full results on MVTec-MAD (Part III)

Method	Binary AD performance						MAD performance		Binary AD performance						MAD performance	
	Level 1	Level 2	Level 3	Level 4	Whole	Ken	C	Level 1	Level 2	Level 3	Level 4	Whole	Ken	C		
bichon_frise																
Skip-GAN [2]	92.80	98.22	85.30	99.95	94.07	0.538	80.08	79.79	89.59	85.74	99.64	88.69	0.549	80.70		
RD4AD [12]	63.99	73.69	78.60	80.36	74.16	0.311	67.37	54.87	61.76	71.06	80.03	66.93	0.290	66.22		
PatchCore [39]	66.82	81.22	79.02	87.93	78.74	0.408	72.78	53.73	74.47	74.92	88.68	72.95	0.396	72.15		
CFLOW-AD [18]	93.38	97.57	97.26	95.72	95.98	0.366	70.46	61.95	86.39	89.37	91.08	82.20	0.438	74.49		
RRD [49]	75.90	87.30	90.52	96.01	87.43	0.523	79.21	65.95	73.51	85.10	97.59	80.54	0.509	78.47		
OCR-GAN [31]	78.46	72.60	69.00	96.58	79.16	0.383	71.40	73.92	75.54	63.97	94.01	76.86	0.339	68.94		
PNI [4]	71.16	82.80	78.79	89.51	80.57	0.413	73.07	64.60	77.04	75.50	90.32	76.87	0.402	72.47		
SPR [46]	61.83	55.24	79.30	71.25	66.90	0.238	63.30	59.69	54.78	80.94	72.90	67.08	0.249	63.92		
IGD [9]	97.67	97.38	96.44	96.92	97.11	0.261	64.60	83.68	92.18	93.70	97.79	91.84	0.489	77.32		
AE4AD [7]	56.96	61.07	34.82	49.49	50.59	0.073	45.94	54.29	61.06	33.86	54.16	50.84	0.037	47.93		
MMAD-4o	98.00	100.0	100.0	100.0	99.50	0.938	95.89	80.56	99.97	100.0	100.0	95.13	0.908	94.90		
MMAD-4o-mini	99.26	99.40	99.40	99.40	99.37	0.622	71.40	75.64	98.80	98.80	98.80	93.01	0.745	81.00		
MMAD-Sonnet	99.36	99.99	100.0	100.0	99.84	0.962	98.29	74.53	97.28	100.0	100.0	92.95	0.911	96.34		
MMAD-Haiku	94.64	99.77	99.88	98.14	98.11	0.790	89.58	66.04	93.43	97.52	93.34	87.58	0.738	87.15		
chinese_rural_dog																
golden_retriever																
Skip-GAN [2]	77.63	88.52	84.17	99.35	87.42	0.526	79.41	66.81	72.34	84.30	98.56	80.50	0.529	79.54		
RD4AD [12]	48.12	63.34	72.42	80.57	66.11	0.331	68.50	44.67	59.42	67.04	74.60	61.43	0.281	65.69		
PatchCore [39]	58.26	79.66	78.19	89.99	76.53	0.429	73.95	55.54	78.62	75.18	88.30	74.41	0.409	72.84		
CFLOW-AD [18]	77.03	94.75	95.91	95.43	90.78	0.491	77.44	69.52	92.76	92.40	93.10	86.94	0.468	76.15		
RRD [49]	69.13	82.34	89.01	97.19	84.42	0.538	80.05	55.54	71.06	80.96	93.14	75.17	0.472	76.40		
OCR-GAN [31]	69.46	72.48	61.81	93.75	74.38	0.342	69.12	69.33	69.22	55.51	90.52	71.14	0.278	65.54		
PNI [4]	60.61	78.41	75.63	89.51	76.04	0.429	73.99	58.47	79.05	73.92	89.60	75.26	0.414	73.15		
SPR [46]	54.94	50.44	77.32	78.32	65.26	0.297	66.60	48.21	45.86	68.97	70.89	58.48	0.241	63.44		
IGD [9]	89.61	95.63	95.35	97.30	94.48	0.468	76.13	90.53	96.75	96.64	97.20	95.28	0.436	74.38		
AE4AD [7]	55.09	60.99	33.96	51.96	50.50	0.052	47.09	47.22	54.46	29.29	45.52	44.12	0.093	44.83		
MMAD-4o	98.80	100.0	100.0	100.0	99.70	0.949	96.62	96.56	100.0	100.0	100.0	99.14	0.936	95.43		
MMAD-4o-mini	99.22	100.0	100.0	100.0	99.80	0.781	82.73	98.26	100.0	100.0	100.0	99.56	0.786	83.51		
MMAD-Sonnet	97.99	99.89	99.89	100.0	99.44	0.952	98.17	92.06	99.82	100.0	100.0	97.97	0.957	98.74		
MMAD-Haiku	90.93	98.35	99.68	99.17	97.03	0.790	90.06	78.53	94.48	97.54	96.36	91.73	0.777	89.71		
labrador_retriever																
teddy																
Skip-GAN [2]	76.06	79.47	90.15	99.03	86.18	0.564	81.53	78.62	85.63	85.93	99.31	87.37	0.541	80.25		
RD4AD [12]	54.06	66.10	74.43	79.77	68.59	0.326	68.23	53.14	64.86	72.71	79.07	67.44	0.308	67.20		
PatchCore [39]	58.63	78.79	77.25	88.94	75.90	0.411	72.96	58.60	78.55	76.91	88.77	75.71	0.410	72.94		
CFLOW-AD [18]	82.99	94.74	94.88	92.81	91.35	0.394	72.00	76.97	93.24	93.96	93.63	89.45	0.431	74.11		
RRD [49]	64.18	77.07	86.42	95.41	80.77	0.509	78.43	66.14	78.26	86.40	95.87	81.67	0.510	78.51		
OCR-GAN [31]	74.02	69.05	68.37	94.94	76.60	0.375	70.97	73.04	71.78	63.73	93.96	75.63	0.343	69.19		
PNI [4]	63.90	79.67	75.30	90.08	77.24	0.409	72.87	63.75	79.39	75.83	89.80	77.20	0.413	73.11		
SPR [46]	59.74	51.80	78.34	65.12	63.75	0.188	60.48	56.88	51.62	76.97	71.70	64.29	0.242	63.55		
IGD [9]	92.81	97.26	97.08	98.44	96.40	0.464	75.92	90.86	95.84	95.84	97.53	95.02	0.424	73.67		
AE4AD [7]	48.71	57.79	31.07	49.07	46.66	0.065	46.38	52.45	59.07	32.60	50.04	48.54	0.064	46.43		
MMAD-4o	95.08	99.90	99.99	100.0	98.74	0.934	96.72	93.80	99.97	100.0	100.0	98.44	0.933	95.91		
MMAD-4o-mini	98.35	100.0	100.0	100.0	99.59	0.780	83.12	94.15	99.64	99.64	99.64	98.27	0.743	80.35		
MMAD-Sonnet	97.28	99.85	99.95	100.0	99.27	0.899	95.15	92.24	99.37	99.97	100.0	97.89	0.936	97.34		
MMAD-Haiku	75.13	94.22	97.88	95.59	90.70	0.739	86.27	81.05	96.05	98.50	96.52	93.03	0.766	88.55		
mean																

Table 19. Full results on MultiDogs-MAD

Method	Binary AD performance				MAD performance		
	Level 1	Level 2	Level 3	Level 4	Whole	Ken	C
Skip-GAN [2]	52.50	49.33	51.03	52.61	51.36	0.014	50.77
RD4AD [12]	51.96	55.12	66.17	71.94	61.30	0.217	62.14
PatchCore [39]	50.05	54.15	63.27	77.95	61.36	0.259	64.47
CFLOW-AD [18]	50.14	52.10	61.23	77.37	60.21	0.238	63.30
RRD [49]	50.86	55.84	65.77	74.84	61.83	0.243	63.55
OCR-GAN [31]	52.51	55.20	47.89	59.72	53.83	0.054	53.03
PNI [4]	48.09	55.60	66.67	79.66	62.50	0.285	65.94
SPR [46]	47.09	47.15	44.03	47.02	46.32	0.034	48.11
IGD [9]	45.65	48.57	52.24	70.87	54.33	0.170	59.51
AE4AD [7]	48.56	48.17	46.49	55.42	49.66	0.029	51.63
MMAD-4o	49.83	59.86	75.54	77.98	65.80	0.433	67.72
MMAD-4o-mini	49.98	56.50	66.87	80.86	63.55	0.348	66.66
MMAD-Sonnet	47.39	58.13	70.85	83.70	65.02	0.403	69.30
MMAD-Haiku	47.66	48.95	55.20	61.74	53.39	0.125	56.20

Table 20. Full results on DRD-MAD

Method	Binary AD performance						MAD performance		
	Level 1	Level 2	Level 3	Level 4	Level 5	Level 6	Whole	Ken	C
Skip-GAN [2]	68.58	64.48	83.27	91.49	55.52	61.28	68.50	0.006	50.34
RD4AD [12]	79.79	74.50	85.02	81.76	86.21	87.70	83.48	0.219	61.90
PatchCore [39]	72.21	71.98	74.52	74.56	77.75	81.67	76.33	0.200	60.88
CFLOW-AD [18]	68.97	66.65	75.52	72.39	76.27	78.99	74.03	0.180	59.78
RRD [49]	79.35	79.00	80.85	84.08	86.74	89.60	84.36	0.240	63.07
OCR-GAN [31]	78.63	41.79	79.62	63.28	60.57	66.43	65.46	0.038	52.09
PNI [4]	85.23	83.19	87.02	84.81	90.29	92.12	87.96	0.241	63.12
SPR [46]	54.64	41.92	56.87	55.69	59.63	55.69	55.14	0.065	53.51
IGD [9]	78.75	82.62	80.87	82.65	89.20	93.11	85.82	0.312	66.99
AE4AD [7]	68.85	68.75	78.15	71.24	74.75	80.97	74.45	0.189	60.26
MMAD-4o	75.05	80.81	82.28	88.67	93.66	97.02	88.07	0.547	76.94
MMAD-4o-mini	66.17	80.05	75.10	81.69	82.63	86.33	79.58	0.351	66.98
MMAD-Sonnet	77.46	86.60	90.58	95.78	97.11	99.10	92.35	0.601	80.54
MMAD-Haiku	56.65	57.01	59.54	59.60	60.44	61.21	59.42	0.142	54.16

Table 21. Full results on Covid19-MAD

Method	Binary AD performance				MAD performance		
	Level 1	Level 2	Level 3	Whole	Ken	C	
Skip-GAN [2]	99.59	99.94	99.40	99.60	0.406	73.65	
RD4AD [12]	98.71	98.91	99.24	98.94	0.509	79.60	
PatchCore [39]	100.0	99.99	100.0	100.0	0.456	76.57	
CFLOW-AD [18]	99.99	99.94	99.99	99.98	0.389	72.63	
RRD [49]	99.25	99.57	99.85	99.53	0.558	82.48	
OCR-GAN [31]	99.61	99.32	99.58	99.53	0.391	72.76	
PNI [4]	100.0	100.0	100.0	100.0	0.455	76.51	
SPR [46]	90.57	93.59	90.77	91.31	0.335	69.50	
IGD [9]	97.64	96.71	99.03	97.91	0.487	78.34	
AE4AD [7]	99.02	98.37	99.79	99.13	0.505	79.42	
MMAD-4o	99.49	98.75	99.80	99.43	0.694	85.61	
MMAD-4o-mini	99.52	99.90	99.95	99.75	0.653	84.97	
MMAD-Sonnet	99.79	99.80	99.87	99.82	0.610	79.23	
MMAD-Haiku	99.99	99.67	99.78	99.85	0.479	74.19	

Table 22. Full results on SkinLesion-MAD